Atmospheric nitrate export in streams along a montane to urban gradient

Ilann Bourgeois, Joel Savarino, Julien Nemery, Nicolas Caillon, Sarah Albertin, Franck Delbart, Didier Voisin, Jean-Christophe Clement

Atmospheric nitrate export in streams along a montane to urban gradient

Ilann Bourgeois[a,b,§], *Joel Savarino*[a], *Julien Némery*[a], *Nicolas Caillon*[a], *Sarah Albertin*[a], *Franck Delbart*[c], *Didier Voisin*[a], *and Jean-Christophe Clément*[b,d]

[a]Université Grenoble Alpes, CNRS, IRD, Grenoble INP*, IGE, F-38000, Grenoble, France

[b]Université Grenoble Alpes, CNRS, LECA, F-38000, Grenoble, France

[c]Université Grenoble Alpes, CNRS, SAJF, F-38000, Grenoble, France

[d]Université Savoie Mont Blanc, INRA, CARRTEL, F-74200, Thonon-Les Bains, France

* Institute of Engineering Univ. Grenoble Alpes

§ ilann.bourgeois@noaa.gov

Abstract

Nitrogen (N) emissions associated with urbanization exacerbate the atmospheric nitrogen influx to remote ecosystems – like mountains –, leading to well-documented detrimental effects on ecosystems (e.g., soil acidification, pollution of freshwaters). Here, the aim was to evaluate the importance and fate of N deposition in a watershed along a montane to urban gradient, using a multi-isotopic tracers approach ($\Delta^{17}O$, $\delta^{15}N$, $\delta^{18}O$ of nitrate, $\delta^{2}H$ and $\delta^{18}O$ of water). In this setting, the montane streams had higher proportions of atmospheric nitrate compared to urban streams, and exported more atmospheric nitrate on a yearly basis (0.35 *vs* 0.10 kg-N ha^{-1} yr^{-1}). In urban areas, nitrate exports were driven by groundwater, whereas in the catchment head nitrate exports were dominated by surface runoffs. The main sources of nitrate to the montane streams were microbial nitrification and atmospheric deposition whereas microbial nitrification and sewage leakages contributed most to urban streams. Based on the measurement of $\delta^{15}N$ and $\delta^{18}O$-NO_3^-, biological processes such as denitrification or N assimilation were not predominant in any streams in this study. The observed low $\delta^{15}N$ and $\delta^{18}O$ range of terrestrial nitrate (*i.e.*, nitrate not coming from atmospheric deposition) in surface water compared to literature suggests that atmospheric deposition may be underestimated as a direct source of N.

Keywords: Nitrogen, deposition, $\Delta^{17}O$, subalpine, isotope, Lautaret

Highlights

- How is nitrogen deposition reflected in streams NO_3^- exports in the French Alps?
- NO_3^- exports in seven streams along an altitude gradient were monitored for two years.
- NO_3^- isotopic composition ($\Delta^{17}O$, $\delta^{15}N$, $\delta^{18}O$) was analyzed to apportion the sources.
- Up to 21% of NO_3^- in montane streams and 5% in urban streams was unprocessed $NO_{3\,atm}^-$.
- Nitrification of atmospheric and mineralized NH_4^+ was the ubiquitous main NO_3^- source.

1. Introduction

Atmospheric nitrogen (N) deposition has increased 10-fold over the past century, increasingly contributing to the global N availability (Galloway et al., 2004). Anthropogenic activities such as fossil-fuel combustion, agriculture, and fertilizers use are responsible for this increase (Fowler et al., 2015; Galloway et al., 2008; Vitousek et al., 1997), with impacts observed in remote ecosystems (Hastings et al., 2009; Holtgrieve et al., 2011; Preunkert, 2003). High N loading to the environment has been documented for many ecosystems (Aber et al., 1989; Clark et al., 2017; Elser et al., 2009; Matson et al., 2002). To address this issue, global efforts are underway to alleviate N inputs into ecosystems, aiming at "minimizing the consequent harm to humans and the environment" (International Nitrogen Initiative, http://www.initrogen.org).

Nitrate concentrations, and fluxes in soils and streams have often been used to assess the N saturation status in watersheds (Aber et al., 1989; Baron and Campbell, 1997; Lovett and Goodale, 2011). However, N exports in stream depend on multiple parameters such as basin topography (Balestrini et al., 2013; Clow and Sueker, 2000), land-cover (Barnes et al., 2014; Williams et al., 2016) and land-management (Barnes and Raymond, 2010; Burns et al., 2009; Lefebvre et al., 2007). As streams integrate many processes at the watershed scale, understanding the specific sources of NO_3^- is important to (1) evaluate the respective contribution of biological and anthropogenic sources, (2) clarify the fate of deposited N in the environment, and (3) understand the origin and the development of N saturation.

Mountainous ecosystems are particularly sensitive to increased N inputs by atmospheric deposition (Baron et al., 2000, 2005, 2011), as they are historically N-limited (Kaye and Hart, 1997). Critical loads for these ecosystems are among the

78 lowest for pristine environments (Baron et al., 2011; Bowman et al., 2006; Nanus et
79 al., 2017), making them vulnerable to long-range transport of atmospheric N emitted
80 from distant sources (Mast et al., 2014; Wasiuta et al., 2015). Atmospheric deposition
81 of N has been shown to contribute significantly, either directly or indirectly, to year-
82 round NO_3^- exports from mountainous catchments (Hundey et al., 2016; Nanus et al.,
83 2008), typically showing a pulse at spring as soils subsurface NO_3^- reservoirs are
84 flushed by snowmelt water (Kendall et al., 1995; Williams et al., 2009; Williams and
85 Melack, 1991).
86 Atmospheric deposition is also a major source of N to urban areas, which
87 receive much higher loads than adjacent environments (Bettez and Groffman, 2013;
88 Fang et al., 2011; Hall et al., 2014; Rao et al., 2014; Templer et al., 2015). Local and
89 regional emissions and subsequent deposition of fuel-combustion derived NO_x and
90 ammonia (NH_3) are responsible for this pattern (Galloway et al., 2004; Kean et al.,
91 2000). NO_x compounds are oxidized into NO_3^- within hours (Beirle et al., 2011), then
92 scavenged from the atmosphere by wet and dry deposition (Hertel et al., 2012). In
93 the atmosphere, NH_3 is in equilibrium with ammonium (NH_4^+), the other primary
94 component of bulk N deposition. Because of the particular topography of urban
95 basins (extended impervious surface, rapid precipitation runoff), urbanization can
96 lead to high NO_3^- exports in freshwater bodies (Groffman et al., 2004; Riha et al.,
97 2014), with major ecological, economic and health consequences (Dodds et al.,
98 2009).
99 This study aims at evaluating how atmospheric deposition of N is reflected in
100 NO_3^- exports in several streams along a montane to urban gradient in the French
101 Alps. Isotopic ($\Delta^{17}O$, $\delta^{15}N$, $\delta^{18}O$ of nitrate, $\delta^{2}H$ and $\delta^{18}O$ of water) and hydro-
102 chemical techniques were combined to evaluate the drivers of NO_3^- inputs and

removal in all streams. The first hypothesis was that due to a higher contribution from other sources (e.g., sewage, fertilizers) in urban areas compared to the mountains, coupled with higher local atmospheric N inputs, total NO_3^- and atmospheric nitrate ($NO_3^-{}_{atm}$) exports should increase along the gradient. The second hypothesis was that different $NO_3^-{}_{atm}$ export dynamics should be observed in urban streams compare to montane streams, due to different hydrological drivers that need to be determined. To test these hypotheses, (1) NO_3^- concentration and isotopic composition were determined in six streams and one lake, ranging from 2000m above sea level (a.s.l.) to 200m (a.s.l.) in the French Alps, (2) the annual export fluxes of $NO_3^-{}_{atm}$ and total NO_3^- were compared across sites along the gradient, (3) the hydrological drivers of the seasonal variability in $NO_3^-{}_{atm}$ proportion were identified and (4) the additional sources of NO_3^- in each watershed were determined.

2. Methods

2.1 Study site and selected streams

The Romanche Valley, located in the central French Alps, spreads from the Lautaret pass (2058m a.s.l.) down to Grenoble (250m a.s.l.) (Figure S1a and b). The Grenoble conurbation counts around 500 000 inhabitants, and is the biggest alpine metropolis in France.

Six streams and one lake were sampled from the Lautaret pass to Grenoble, draining watersheds of increasing size and with distinct geomorphic and biogeographic characteristics (Table 1). Two alpine streams were sampled at ~2000m a.s.l.. These drain the South exposed side of the Lautaret pass (S-upper montane, n = 157) and the North exposed side (N-upper montane, n=93), where for the latter the stream is mainly fed by glacier melt (Figure S1c). The mid montane stream (n=67) was sampled at ~1600 m a.s.l., 6km down from the Lautaret pass (Figure S1c). All three streams are tributaries of Romanche (lower montane stream, n=127) that was sampled 15km down from the Lautaret pass at ~1000m a.s.l., before ending in Chambon lake (Figure S1d). The lake (~ 900m a.s.l., n=29) is an artificial reservoir managed by the French national electricity company (EDF), 21km down from the Lautaret pass. The two urban streams (~210 m a.s.l.) were located, for one, upstream from Grenoble main urbanized area (upper urban stream, n=48) and, for the other, downstream (lower urban stream, n=45), and were separated by 8km (Figure S1e). The lower urban stream waters are derived from the lower montane stream (and the lake). The upper urban stream, Isère, has surface water from another alpine valley. The upper urban stream flows through residential areas, gardens, and some arable fields prior to the sampling location whereas the lower

urban site abuts industrial developments as well as residential neighborhoods (Dutordoir, 2014).

2.2 Deposition and streams sampling, discharge and conductivity

Atmospheric wet and dry deposition samples were collected using a WADOS Kroneis collector (GmbH Austria) at the S-upper montane site from April 2016 to April 2017. A moving lid – connected to heated moisture sensor – ensured the separated collection by covering alternatively the dry funnel (under rain or snow conditions) and the wet funnel (the rest of the time). The deposition collector was installed on the roof of the Lautaret pass Alpine Research Station (~210 m a.s.l.), https://www.jardinalpindulautaret.fr) to reduce the impact of ground turbulence and input of soil particles. Samples were collected approximately every three weeks. Precipitation samples were kept at 4°C during the sampling period, then frozen until further analysis. After exposure to the atmosphere, the dry deposition funnel was rinsed with 500 mL of MilliQ water, and the sample was stored at -20°C.

Stream and lake water was sampled at all sites according to the Niwot Ridge LTER protocol (Williams and Melack, 1991). In short, samples (total n = 566) were collected manually in 1L Nalgene bottles, previously washed 3 times with MilliQ water (18.2 $M\Omega.cm^{-1}$ at 25°C) and rinsed three times with stream water before collection. All samples were then kept at -20°C until further treatment. Water samples were collected on a weekly to monthly basis from January 2015 to December 2016, with increased sampling frequency in two of the upper tributaries from April to May 2016. During this intensive sampling period, water was collected using three automatic water samplers (Teledyne ISCO® 3700) every two or three hours at the S-upper and lower montane sites. Water conductivity, shown to be a good proxy of discharge

(Weijs et al., 2013), and water temperature were also intensively monitored (2 minutes stepwise) over that period using CTD-Diver® sensors. Spring sampling was sporadic in the N-upper montane site because of persistent snow cover. Winter sampling was not possible at the lake site as it was frozen.

Discharge data was obtained from the national discharge-monitoring network (Banque Hydro) or measured every hour for both lower montane and urban site. Stream stage at the upper urban site was monitored every 30 minutes using water level gauge sensor (OTT®) at Grenoble Campus station (more details in Mano, 2008; Némery et al., 2013). Discharge was estimated from stage measurements by using rating curve (water level *vs* discharge) (Némery et al., 2013). Continuous discharge could not be measured at the upper and mid montane sites due to the torturous nature of the streams. Precipitation data were obtained from the Alpine Mountain Meteorological Office Network (www.romma.fr) at the upper montane site and using a rain gauge (Précis Mécaniques®) on a building roof of the Grenoble Campus, close to the upper urban site.

2.3 Chemical and isotopic analysis

All stream and deposition samples were left to unfreeze at ambient temperature prior to being filtered using 0.45µm Whatman GD/X syringe filters linked to a peristaltic pump. They were subsequently analyzed for ion concentrations ($[NH_4^+]$, $[NO_3^-]$, $[SO_4^{2-}]$, $[Cl^-]$, $[Ca^{2+}]$) using a colorimetric technique (Gallery Plus, Thermo Fisher Scientific, Waltham, Massachusetts, USA). An analytical error <0.01 mg L^{-1} was determined for all ions based on the standard deviation of commercial control solutions (ThermoFisher®) analyzed as unknowns. Major ions such as sulfate and calcium and chloride are often used as hydro-chemical tracers of water

flowpaths or water sources (Briand, 2014; Devito et al., 2000; Hall et al., 2016; Stoewer et al., 2015), and were measured to identify the dominating hydrological regimes in the studied sites.

All samples were concentrated on an anionic resin (0.6mL AG 1-X8 resin, Cl^--form, Bio-Rad) with recovery efficiency over 98.5% (Erbland, 2011) and eluted with 10mL of a 1M NaCl solution for isotopic analysis (Templer and Weathers, 2011). Isotopic analyses of NO_3^- ($\Delta^{17}O$, $\delta^{18}O$ and $\delta^{15}N$) were conducted on an MAT 253 IRMS using an adapted version of the denitrifier method (Kaiser et al., 2007; Morin et al., 2008). More details about the experimental setup can be found elsewhere (SI Text). The analytical errors – calculated as the standard deviation of the residuals from the linear regression between raw data of the reference standards (USGS 32, USGS 34 and USGS 35) and their accepted values – were ± 0.4, 1.5 and 0.3‰ for $\Delta^{17}O$, $\delta^{18}O$ and $\delta^{15}N$ of NO_3^-, respectively. Slopes and intercepts of the linear regressions are then used to convert raw sample data into calibrated values (VSMOW scale for O isotopes, and N2-air scale for N isotopes).

A subset of stream, rain, and snow samples (collected in winter 2015-2016) were sent for δ^2H and $\delta^{18}O$ analyses on a Picarro L2130-i at the Laboratoire des Sciences et du Climat (LSCE) in Paris, France. The analytical error – inferred from the replicate analysis of internal standards calibrated against V-SMOW2 et V-SLAP2 standards – was ± 0.7 and 0.2 ‰ for δ^2H and $\delta^{18}O$ of H_2O, respectively.

2.4 NO_3^- sources apportionment

A number of previous studies have used the dual isotope approach ($\delta^{18}O$ and $\delta^{15}N$ of NO_3^-) to track the spatio-temporal variability of sources contribution to NO_3^- pools in a large variety of environmental matrixes (Campbell et al., 2002; Durka et al.,

1994; Elliott et al., 2009; Yang and Toor, 2016). Biochemical processes such as denitrification or assimilation have also been shown in laboratory experiments to distinguishably enrich residual NO_3^- in heavier isotopes, here ^{15}N and ^{18}O (Granger et al., 2004, 2010; Treibergs and Granger, 2017), although this enrichment can be diluted by newly nitrified NO_3^- with low N and O isotopic values (Granger and Wankel, 2016; Mayer et al., 2002). Environmental studies also reported characteristic NO_3^- isotopic enrichment for denitrification (Clément et al., 2003; Fang et al., 2015; Wexler et al., 2014), assimilation (Emmerton et al., 2001; Estrada et al., 2017; X.-Y. Liu et al., 2013) or photolysis (Frey et al., 2009; Shi et al., 2015; Ye et al., 2016). However, the isotopic fingerprint of biological processes can lead to inaccurate NO_3^- source apportionment in some cases, especially in delineating the respective contribution of the microbial and the atmospheric sources (Michalski et al., 2004; Riha et al., 2014; Rose et al., 2015a).

In the past few years, a growing number of studies have used an isotopic particularity of $NO_3^-_{atm}$ to quantify the contribution of atmospheric deposition to terrestrial N pools (Costa et al., 2011; Hundey et al., 2016; Tsunogai et al., 2014). $NO_3^-_{atm}$ is enriched in ^{17}O due to its production pathways (*i.e.*, oxidation of NO_x by O_3), showing a deviation from the Terrestrial Fractionation Line (Thiemens, 2006). $\Delta^{17}O$ is a quantification of this deviation, calculated as $\Delta^{17}O = \delta^{17}O - 0.52 * \delta^{18}O$ in the present work. $\Delta^{17}O$ value of $NO_3^-_{atm}$ generally ranges between 20 and 35‰ in temperate latitudes (Morin et al., 2009; Savarino et al., 2007), whereas $\Delta^{17}O$ value of NO_3^- from all other sources (industrial fertilizers, nitrification) or of biologically processed $NO_3^-_{atm}$, is 0‰ (Michalski et al., 2004, 2015). In this study, these two distinct $\Delta^{17}O$ values were used as end-members in a simple mixing model to quantify unprocessed $NO_3^-_{atm}$ proportion (f_{atm}) in streams, according to Michalski et al.

(2004):

(Eq. 1) $$f_{atm} = (\Delta^{17}O\text{-}NO_3^-{}_{sample} / \Delta^{17}O\text{-}NO_3^-{}_{atm})$$

The atmospheric fraction (f_{atm}) and the terrestrial fraction of NO_3^- (f_{ter} = 1 - f_{atm}) can be used to remove the isotopic influence of $NO_3^-{}_{atm}$ on samples, and allow for a better interpretation of biological processes that affect $\delta^{15}N$ and $\delta^{18}O$ (Dejwakh et al., 2012; Michalski et al., 2004; Riha et al., 2014; Tsunogai et al., 2010). $\delta^{18}O$ *vs* $\delta^{15}N$ plots have been intensively used to evaluate sources of N and potential processes (denitrification, assimilation) in the environment (Burns et al., 2009; Durka et al., 1994; Griffiths et al., 2016; Kendall et al., 1995; X.-Y. Liu et al., 2013). However, because of strongly distinct $\delta^{18}O\text{-}NO_3^-{}_{atm}$ values compared to $\delta^{18}O\text{-}NO_3^-{}_{ter}$, even a low f_{atm} can lead to scatter in a dual-isotope plot. Removing the atmospheric $\delta^{15}N$ and $\delta^{18}O$ components from environmental samples leads to an easier assessment of biological processes, such as assimilation or denitrification. This isotope correction was applied on the samples using the isotopic mass balances from Riha et al. (2014):

(Eq.2) $$\delta^{18}O_{ter} = (\delta^{18}O_{sample} - \delta^{18}O_{atm} * f_{atm}) / f_{ter}$$

(Eq.3) $$\delta^{15}N_{ter} = (\delta^{15}N_{sample} - \delta^{15}N_{atm} * f_{atm}) / f_{ter}$$

$\delta^{15}N_{atm}$ and $\delta^{18}O_{atm}$ were inferred from NO_3^- in wet and dry atmospheric deposition (see section 3.2). A formal propagation of uncertainty was performed to assess the error associated with individual values of f_{atm}, $\delta^{18}O\text{-}NO_3^-{}_{ter}$ and $\delta^{15}N\text{-}NO_3^-{}_{ter}$. Although

the error associated with individual values can be large (Figure S2), averaging across samples throughout the year results in a robust estimate of annual f_{atm}, $\delta^{18}O\text{-}NO_3^-{}_{ter}$ and $\delta^{15}N\text{-}NO_3^-{}_{ter}$ values (Dejwakh et al., 2012).

2.5 Fluxes of NO_3^- and $NO_3^-{}_{atm}$

NO_3^- yields (F_m in kg-N w^{-1}) were calculated at each site – when possible – on a weekly basis using the mean weekly discharge (Q_m in m^3 s^{-1}) and instantaneous concentrations ($[NO_3^-]_i$ in mg-N L^{-1}), as follows:

(Eq.4) $$\mathbf{F_m = Q_m * [NO_3^-]_i}$$

Total specific annual stream loads of NO_3^- (F_{tot} in kg-N ha^{-1} yr^{-1}) were calculated as the annual sum of weekly NO_3^- exports during the study period (2015 and 2016), as follows:

(Eq.5) $$\mathbf{F_{tot} = (\sum_m Fm) \,/\, (watershed\ area)}$$

Finally, total annual $NO_3^-{}_{atm}$ loads (F_{atm}) were calculated for each year by multiplying the total annual stream yield of NO_3^- (F_{tot}) by the discharge-weighted annual mean f_{atm} in the stream (see Eq. 1), according to Tsunogai et al. (2014, 2010):

(Eq. 6) $$\mathbf{F_{atm} = F_{tot} * f_{atm}}$$

When $[NO_3^-]$ or $\Delta^{17}O$ values were not available for a given date (n=4, 2 and 2 for the lower montane, upper urban and lower urban streams, respectively), they were

290 replaced by the mean [NO_3^-] or $\Delta^{17}O$-NO_3^- values measured on the previous and the
291 following dates, to capture temporal variations due to hydrological events. Note that
292 the use of instantaneous [NO_3^-] to calculate weekly streams NO_3^- loads might over or
293 under estimate the real NO_3^- yield in streams.
294
295 **2.6 Statistical analysis**
296 A Mann-Whitney test was applied to surface water data to determine whether
297 mean concentrations and isotopic values were significantly different between
298 streams. A Spearman test was applied to evaluate the correlation between stream
299 water parameters (typically $\Delta^{17}O$, $\delta^{18}O$, $\delta^{15}N$ and ion concentrations). Differences
300 and correlations were considered significant when the *p* value was ≤0.05. All
301 statistical analyses were conducted using R software (v3.2.3). Unless specified
302 otherwise, the uncertainty accompanying the mean values is the standard deviation.
303
304 **3. Results**
305 **3.1 Precipitation and discharge**
306 Cumulated precipitation was 537 and 609mm in 2015 and 804 and 740mm in
307 2016 at the upper montane and the urban sites, respectively. Discharge at the lower
308 montane site reflects a snowmelt influenced hydrological regime. It peaked up to 30
309 $m^3\ s^{-1}$ in spring, and was significantly higher from April to October compared to the
310 rest of the year. Discharge at both urban sites was consistent with a hydrological
311 regime driven by snowmelt in spring-summer (main maximum), and rainfall in autumn
312 (secondary maximum), a dual contribution similar to what was obtained in the
313 Colorado Front Range (Cowie et al., 2017). At the upper urban site, discharge
314 peaked at 900 $m^3\ s^{-1}$, whereas maximum discharge was 300 $m^3\ s^{-1}$ at the lower

315 urban site, a difference due to the streams draining two distinct watersheds (Figure
316 S3).
317
318 **3.2 Comparison of dissolved solutes across sites**
319 Solutes concentration varied by up to 3 orders of magnitude among
320 precipitation and streams samples (Table S2 and Figure 1). [NH_4^+] was low in both
321 dry and wet deposition at the S-upper montane site, and mostly (>90%) under the
322 detection limit (<0.02 mg L^{-1}) in all streams. [NO_3^-] was significantly higher in rain
323 samples compared to stream samples. The highest annual mean [NO_3^-] was
324 measured in the lower urban stream (1.4 ± 0.5 mg L^{-1}) and the lowest in the S-upper
325 montane stream (0.2 ± 0.2 mg L^{-1}). [NO_3^-] at the N-upper montane, mid montane,
326 lower montane and upper urban sites were not statistically different (1.4 ± 1.3, 1.1 ±
327 0.6, 1.0 ± 0.6 and 1.1 ± 0.4 mg L^{-1}, respectively). [SO_4^{2-}] and [Ca^{2+}] were both very
328 low in precipitation relative to streams. The S-upper montane stream exhibited the
329 highest annual mean [SO_4^{2-}] and [Ca^{2+}] (98.5 ± 39.5 and 44.5 ± 18.2 mg L^{-1},
330 respectively), followed by the upper urban stream (74.1 ± 26.9 and 35.2 ± 13.1 mg L^{-1}
331 , respectively), and the lowest concentrations were measured at the N-upper
332 montane site (22.1 ± 35.9 and 16.5 ± 16.0 mg L^{-1}, respectively). [Cl^-] was very low in
333 precipitation samples and in most montane streams (mean values all < 3 mg L^{-1}),
334 respectively. Higher annual mean [Cl^-] were measured in the urban streams (4.7 ±
335 1.8 and 16.6 ± 12.3 mg L^{-1} for the upper and lower urban stream, respectively).
336
337 **3.3 Isotopic composition of NO_3^- in precipitation and streams**
338 Mean annual $NO_{3\,atm}^-$ isotopic values (Table S1) were non-significantly higher
339 in dry deposition than in wet deposition (significant only for δ^{15}N-NO_3^-), a pattern

widely monitored at temperate latitudes (Beyn et al., 2014; Freyer, 1991; Mara et al., 2009). Mean and associated standard deviation of $\Delta^{17}O\text{-}NO_3^-$ in precipitation and dry deposition were 26.4 ± 3.2 and 24.7 ± 3.5 ‰, respectively. These values are in the same range as previously reported data for $\Delta^{17}O\text{-}NO_{3\,atm}^-$ (Costa et al., 2011; Michalski et al., 2004; Tsunogai et al., 2010, 2016). The mean $\Delta^{17}O$ value for total deposition was 25.6 ± 3.3 ‰, and was used to quantify the atmospheric component of NO_3^- pools in streams (see section 2.4, Eq. 1). Mean annual total $\delta^{18}O\text{-}NO_{3\,atm}^-$ (70.8 ± 7.2 ‰) and $\delta^{15}N\text{-}NO_{3\,atm}^-$ (-4.8 ± 5.9 ‰) are also consistent with a reservoir of exclusively $NO_{3\,atm}^-$ (Kendall et al., 2007), and these values were used to correct samples from their atmospheric $\delta^{18}O$ and $\delta^{15}N$ components (see section 2.4, Eq.2 and 3).

Significantly higher annual mean $\Delta^{17}O\text{-}NO_3^-$ was measured in montane streams compared to urban streams, with the exception of the mid montane site (1.0 ± 0.7 ‰), which exhibited the lowest values (Figure 2a). Both upper and lower urban, along with the mid montane streams were also characterized by the highest annual mean $\delta^{15}N\text{-}NO_3^-$ (3.7 ± 1.0 ‰, 4.9 ± 5.6 ‰ and 4.0 ± 2.0 ‰, respectively) (Figure 2c). The lake, fueled by the lower montane stream, presented the highest annual mean $\Delta^{17}O\text{-}NO_3^-$ (5.1 ± 1.8 ‰) and $\delta^{18}O\text{-}NO_3^-$ (8.6 ± 6.2 ‰), and the lowest $\delta^{15}N\text{-}NO_3^-$ (-0.2 ± 2.4 ‰) (Figure 2a, b and c). It must be stressed out again that the lake was only sampled when unfrozen (*i.e.*, late spring, summer and autumn), potentially biasing NO_3^- mean isotopic values at this site.

3.4 Trends in isotope composition of NO_3^- across sites

Seasonal variations of stream NO_3^- isotopes and corresponding f_{atm} are shown in Figure 3. The three montane streams followed a similar pattern of seasonal variations in 2015 and 2016. At the S-upper montane site, $\Delta^{17}O\text{-}NO_3^-$ and $\delta^{15}N\text{-}NO_3^-$ were significantly negatively correlated, with brief but high $\Delta^{17}O\text{-}NO_3^-$ peaks in spring, followed by a slow but continuous increase peaking late summer/beginning of autumn. At the N-upper site, a saw tooth pattern in summer and autumn occurred right after a small but temporally wider increase at snowmelt, in early summer. $\Delta^{17}O\text{-}NO_3^-$ and $\delta^{15}N\text{-}NO_3^-$ in the mid montane stream presented little variations throughout the seasons, apart from a raise in $\delta^{15}N\text{-}NO_3^-$ in spring/summer 2016. $\Delta^{17}O\text{-}NO_3^-$ and $\delta^{15}N\text{-}NO_3^-$ were significantly negatively correlated in the lower montane stream and in the lake, with significantly higher $\Delta^{17}O\text{-}NO_3^-$ from April to October – relative to the rest of the year – in a very similar way to discharge (Figure S3). Finally, $\Delta^{17}O\text{-}NO_3^-$ and $\delta^{15}N\text{-}NO_3^-$were not correlated and did not vary much in urban streams, except for some occasional high $\delta^{15}N$ peaks in spring and winter 2015 at the lower urban site.

4. Discussion

4.1 NO_3^- exports in streams

4.1.1 $[NO_3^-]$ across the altitude gradient

There were little differences in streams $[NO_3^-]$ along the elevation gradient despite an expected higher contribution from anthropogenic activities to streams N pool closer to urbanized areas (Groffman et al., 2004; Tsunogai et al., 2016). The 0.2-1.4 mg L^{-1} mean $[NO_3^-]$ range at the montane sites is consistent with the 0.6-1.6 mg L^{-1} range in other Alpine valleys (reviewed in Balestrini et al., 2013), and the 0.9-1.5 mg L^{-1} range in elevated sites of the Colorado Front Range (Baron and Campbell, 1997; Campbell et al., 1995). The N-upper montane site had a much wider $[NO_3^-]$

range than the S-upper montane site, which is attributed to glacier melt influence (Barnes et al., 2014; Williams et al., 2007). [NO_3^-] in urban streams was low when compared to other concentrations measured in urban settings, such as the Tucson basin where values up to 62 mg L^{-1} were determined (Dejwakh et al., 2012) or up to 26 mg L^{-1} in the Gwynns Falls watershed (Groffman et al., 2004).

4.1.2 $NO_3^-{}_{atm}$ contribution to total NO_3^-

Atmospheric deposition contributed significantly more to NO_3^- pool in streams at the montane sites relative to the urban sites – exception being the mid montane site (Figure 2). The Chambon lake showed the highest f_{atm}, although it is possible that sampling of this reservoir exclusively in summer resulted in a biased estimate of mean annual $NO_3^-{}_{atm}$. High $NO_3^-{}_{atm}$ inputs in montane streams (up to 47%) clearly outline the influence of the melting snowpack releasing its load of atmospheric nitrate (see section 4.2.1), as widely reported elsewhere (Kendall et al., 1995; Ohte et al., 2004; Pellerin et al., 2012; Tsunogai et al., 2014, 2016). The mid montane stream exported the lowest proportion of $NO_3^-{}_{atm}$. Smoother topography gradient on this watershed (slopes are 17%, Table 1) can account for this by impeding direct runoff to stream during hydrological extremes (e.g., snowmelt), thus exerting a strong control over NO_3^- isotopic values in the stream (Balestrini et al., 2013; Clow and Sueker, 2000). In addition, a smoother topography gradient also drives a higher $NO_3^-{}_{atm}$ residence time in soils that would overwrite its $\Delta^{17}O$ signature when recycled by microorganisms. The low f_{atm} in urban streams is dissimilar to others results that have shown an increasing f_{atm} in streams along an urbanization gradient (Riha et al., 2014), or high $NO_3^-{}_{atm}$ inputs in urban runoff (Yang and Toor, 2016). In urban areas, the combination of more impervious surface area coupled to higher atmospheric

414 deposition inputs is a strong driver that was expected to promote a higher proportion
415 of $NO_3^-{}_{atm}$ in urban streams, relative to montane sites. Indeed, NO_3^- atmospheric
416 concentrations in Grenoble's urban area are 10 to 100 times higher than atmospheric
417 concentrations observed at the Lautaret pass (Bourgeois, 2017; Tomaz et al., 2017),
418 which should have promoted higher $NO_3^-{}_{atm}$ loads in urban streams. However, higher
419 total $NO_3^-{}_{atm}$ loads are calculated at the lower montane site where $NO_3^-{}_{atm}$
420 represented 21% of the total annual NO_3^- exports (Table 2).
421 Elevated N deposition in the Alps – also illustrated by higher [NO_3^-] in wet and
422 dry deposition compared to streams (Table S2) – is a well-documented phenomenon
423 (Kirchner et al., 2014; Rogora et al., 2006). Sustained nitrogen deposition in addition
424 to the steep slopes of the lower montane watershed (Table 1) can account for the
425 higher total $NO_3^-{}_{atm}$ flux at the montane site. Grenoble conurbation land cover is
426 mainly constituted of forest and lower vegetation (64%) followed by agricultural fields
427 (24%), and impervious surfaces (10%) are only a minor surface occupation (UE-
428 SOeS, CORINE Land Cover, 2006). $NO_3^-{}_{atm}$ inputs are thus likely to move to multiple
429 sinks, be biologically recycled or lost *via* different processes (e.g., denitrification,
430 photolysis (Clément et al., 2003; Ye et al., 2016)) before being collected by the urban
431 streams (Rao et al., 2014). Furthermore, a strong decoupling between atmospheric N
432 deposition and urban soils N cycling has recently been proposed, pointing at a
433 distinct urban biogeochemical N cycle – that entails that land-management practice,
434 not N deposition, is the ultimate driver of N cycling – and that would need further
435 investigation (Decina et al., 2017). Additionally, in France urban rainwater and
436 domestic wastewater are traditionally collected in the same pipe system before being
437 purified in a sewage treatment plant downstream of the cities. This would also limit
438 direct rainwater runoff to the streams, as illustrated by the statistically similar [NO_3^-] in

urban streams compared to montane streams (Figure 1). One, or a combination of several of these factors would lower $NO_3^-{}_{atm}$ exports in urban streams, even lower than montane streams $NO_3^-{}_{atm}$ exports in this case. Therefore, the low f_{atm} in urban streams certainly reflects the recycling and replacement of $NO_3^-{}_{atm}$ by terrestrial NO_3^- sources along the smoother topography gradient, in a similar way to the mid-montane stream.

4.2 Links between hydrology, topography and $NO_3^-{}_{atm}$ exports

4.2.1 Seasonal variations of $NO_3^-{}_{atm}$ proportion in streams

Seasonal variations of $NO_3^-{}_{atm}$ exports at the montane sites reflected the influence of hydrologic and topographic features of the basins, and are thoroughly discussed elsewhere (Bourgeois, 2017). The S-upper montane site exports are governed by quick runoff to streams in the early stages of spring, followed by a diffuse resurgence of infiltrated snowmelt water in summer and autumn. The period between these two event lasts about 5 months both in 2015 and in 2016, an indicator of either the water transit time in the calcareous substrate of the watershed or of the aquifer refill time before flushing to the stream. The N-upper montane stream is fueled by glacier melt, leading to higher $[NO_3^-]$ than its southern counterpart by 1 order of magnitude (Figure 1). This is a consequence of the permafrost thawing at that site (Bodin et al., 2009), thus increasing nitrification and/or mobilization of stored N from disturbed soils (Barnes et al., 2014; Hood and Scott, 2008; Louiseize et al., 2014). Occasional higher f_{atm} at the N-upper site are triggered by rainstorm events (Figure S3). The lower montane stream and the lake had very similar seasonal variations of $\Delta^{17}O\text{-}NO_3^-$, featuring the gradual melting of upstream snowpack throughout the growing season (May to October). The mid montane and the urban

streams showed no marked seasonal variation, because of the buffering effect of soils and the higher N cycling rates inherent to more intensive land management treatments that prevented $NO_3^-{}_{atm}$ inputs to streams (Table 1).

4.2.2 Groundwater and surface runoff respective influence $NO_3^-{}_{atm}$ proportion in streams

Significant correlations between rock-derived solutes (SO_4^{2-} and Ca^{2+}) in all streams (Figure S4) indicate groundwater contribution to streams as a unifying feature along the montane to urban gradient. Varying concentrations of rock-derived solutes are in good agreement with the geologic characteristics of each watershed (*i.e.*, highest concentrations in the S-upper montane and the upper urban streams draining calcareous basins, lowest concentrations in the N-upper montane stream draining a less erodible bedrock, see Table 1 and Figure 1). In this study, year-round detectable $\Delta^{17}O\text{-}NO_3^-$ translate the continuous $NO_3^-{}_{atm}$ exports in all streams (Figure 3), even during baseflow when streams are mostly fueled by groundwater. Most studies focusing on NO_3^- dynamics in runoff reported $NO_3^-{}_{atm}$ only during stormflow or snowmelt periods (Burns et al., 2009; Campbell et al., 2002; Pellerin et al., 2012). However, these studies used the dual isotope approach (*i.e.*, $\delta^{18}O$ and $\delta^{15}N$ of NO_3^-), which does not account accurately for $NO_3^-{}_{atm}$ in streams compared to the $\Delta^{17}O$ tracer (Michalski et al., 2004; Rose et al., 2015a). In a growing body of work using $\Delta^{17}O\text{-}NO_3^-$ in streams, $NO_3^-{}_{atm}$ presence during baseflow is a unifying feature (Rose et al., 2015a; Sabo et al., 2016; Tsunogai et al., 2016). In all these studies, f_{atm} ranged from 1-12% in baseflow, except for a coniferous watershed in West Virginia, which led to f_{atm} of 54% in stream, due to low sampling resolution (n=4). Here, f_{atm} ranged from 1-20% (with a median associated error of 3%, Figure S2) in all streams

during the dormant season (in grey, Figure 3), somewhat higher than the literature data range – because of the extended influence of snowmelt in mountainous sites during the growing season. The high $\Delta^{17}O\text{-}NO_3^-$ peaks at the S-upper montane site in March 2015 are due to a shorter winter this year.

However, even if groundwater contributed at all sites to streams water, its influence on streams ionic exports had most impact in the urban reaches. No or near static correlations between either NO_3^- isotopes or conservative ions and discharge (Figure 4) imply that a geochemically equilibrated groundwater reservoir dominates stream exports at the urban sites, instead of surface runoff (Hall et al., 2016). Oppositely, $\Delta^{17}O\text{-}NO_3^-$ increased significantly with discharge at the lower montane site, highlighting the influence of snowmelt on $NO_{3\,atm}^-$ exports (Figure 4a). Decreasing weathering products concentrations with high flow also evidence the decreasing contribution of groundwater towards more surficial water at snowmelt (Figure 4d and f). No significant correlation of $[NO_3^-]$ with discharge in any stream implies a homogenized NO_3^- pool in groundwater reservoirs by infiltrated snowmelt inputs. In line with this hypothesis, a dual isotope plot of water illustrates that snowmelt more than rain fueled the streams, even down to the outskirts of Grenoble (Figure S5). Other studies also reported similar findings of underground reservoirs fed by snowmelt in mountains vicinity (Brooks et al., 1999; Hall et al., 2016; Williams et al., 2009).

4.2.3 A focus on snowmelt period in montane streams

The intensive sampling campaign in spring 2016 at the S-upper montane and the lower montane sites provided no evidence of diurnal pattern for any solutes in the streams (data not shown). However, $\Delta^{17}O\text{-}NO_3^-$ did follow a diurnal pattern at the S-

upper montane site, a pattern not seen in the lower montane stream (Figure S6a). Conductivity (at both sites) and discharge (lower montane site only) showed very pronounced diurnal variations, highlighting the hydrological influence of snowmelt during the day (Figure S6b and c), also consistent with previous studies in the same location (Mano et al., 2009). At the lower montane site, discharge and conductivity were negatively correlated (Figure 5d), as their diurnal variations were driven by distinct hydrological regime (*i.e.*, baseflow for conductivity, snowmelt for discharge). That conductivity is controlled by baseflow is also supported by significant positive correlations between weathering solutes and conductivity at the S-upper montane site (Figure 5c). Therefore, assuming a similar relationship between conductivity and discharge is true at the S-upper montane stream, and considering that conductivity and $\Delta^{17}O\text{-}NO_3^-$ were also negatively correlated (Figure 5a), snowmelt-induced discharge in daytime is certainly the driver of the diurnal variations of $NO_{3\,atm}^-$ exports. Oppositely to another study showing in stream diurnal $[NO_3^-]$ variations at snowmelt in northern Vermont (Pellerin et al., 2012), no significant temporal trend in any of the two streams was observed here. Yet, the lower montane stream was only on the rising limb of discharge when sampled, at the very beginning of the snowmelt period. Therefore, the absence of observed diurnal cycle at this site at this time may not be representative of day-night variations later in the season.

4.3 Isotopic composition of $NO_{3\,ter}^-$

4.3.1 NH_4^+ nitrification is the main source of $NO_{3\,ter}^-$ in all streams

Isotopic values of $NO_{3\,ter}^-$ (*i.e.*, NO_3^- corrected from the atmospheric component accordingly to Eq. 2 and 3) are reported in a dual isotope ($\delta^{18}O$ and $\delta^{15}N$) plot in Figure 6. This allows the evaluation of the respective contribution of terrestrial

sources of $NO_3^-{}_{ter}$ to streams. Here, most $\delta^{15}N\text{-}NO_3^-{}_{ter}$ in streams span a 0 to 7‰ range, delineating nitrification of NH_4^+ as the main source of stream $NO_3^-{}_{ter}$ contents (Figure 6). This is in line with watersheds land cover consisting principally in natural or semi-natural vegetation (Table 1), where NO_3^- fertilizers are rarely used. Only very few samples (n = 4) had both $\delta^{15}N\text{-}NO_3^-{}_{ter}$ and $\delta^{18}O\text{-}NO_3^-{}_{ter}$ characteristic of NO_3^- fertilizers. It is complicated to segregate the substrate of nitrification (*i.e.*, deposited atmospheric NH_4^+ ($NH_4^+{}_{atm}$) or mineralized soil NH_4^+ ($NH_4^+{}_{org}$)) that led to the production of $NO_3^-{}_{ter}$ in streams. Indeed, nitrification of $NH_4^+{}_{atm}$ and $NH_4^+{}_{org}$ produces NO_3^- with overlapping $\delta^{15}N$ ranges (Kendall et al., 2007). However, a fraction of samples, mostly from montane streams, had $\delta^{15}N\text{-}NO_3^-{}_{ter}$ lower than 0‰, consistent with nitrification of $NH_4^+{}_{atm}$ (Kendall et al., 2007; T. Liu et al., 2013).

4.3.2 Biological removal of NO_3^- was not predominant in any stream

Weak negative correlations between $\delta^{18}O\text{-}NO_3^-$ and $\delta^{15}N\text{-}NO_3^-$ at all sites, exception made of the lower urban site, indicate that biological processes such as denitrification or assimilation do not control NO_3^- cycling in streams. Indeed, such processes, if dominant, should enrich residual $\delta^{18}O\text{-}NO_3^-$ and $\delta^{15}N\text{-}NO_3^-$ along a positively correlated line (Granger et al., 2008, 2010; Kendall et al., 2007), in a similar fashion to what is observed at the lower urban site. Yet, that $\delta^{15}N\text{-}NO_3^-$ was significantly correlated to [Cl^-] in this stream (data not shown) rather proves that the high $\delta^{15}N\text{-}NO_3^-$ values are due to interception of sewage-originated wastewater (Hall et al., 2016). Decreasing $\delta^{15}N\text{-}NO_3^-$ and [Cl^-] with discharge (Figure 4b and e) at this specific site also supports a groundwater origin of these nitrate pollution episodes.

4.3.3 Low $\delta^{18}O\text{-}NO_3^-{}_{ter}$ calls for a more systematic use of the $\Delta^{17}O$ tracer

564 $\delta^{18}O\text{-}NO_3^-{}_{ter}$ values as low as -20‰ were obtained after removing the
565 atmospheric imprint (Figure 6 and Figure S7). The mean $\delta^{18}O\text{-}NO_3^-{}_{ter}$ ranged
566 between -6.3 and -8.0‰ in the mountainous streams, significantly lower than
567 previously reported values of terrestrial $\delta^{18}O\text{-}NO_3^-$ in freshwater systems (from -2.9 to
568 -4.2‰ in Tsunogai et al. (2016, 2014, 2010)) or produced through in vitro incubation
569 experiments (> 0‰ in Burns and Kendall (2002), Mayer et al. (2001) and Spoelstra et
570 al. (2007)).The mean $\delta^{18}O\text{-}NO_3^-{}_{ter}$ range between -2.6 and -2.8‰ in the urban
571 streams, far lower than values > 9‰ inferred in other urban areas (Riha et al., 2014)
572 or mostly positive values in a semiarid urban setting (Dejwakh et al., 2012).
573 The theoretical range for $\delta^{18}O\text{-}NO_3^-{}_{nit}$ (*i.e.*, theoretical $\delta^{18}O\text{-}NO_3^-$ after
574 nitrification) is -15 to 15‰, assuming soil-water and O_2 respectively contribute to NO_3^-
575 -O accordingly to $\delta^{18}O\text{-}NO_3^- = 1/3\ (\delta^{18}O\text{-}O_2) + 2/3\ (\delta^{18}O\text{-}H_2O)$ (Kendall et al., 2007).
576 Here, a subset of 5 snow-water samples and 2 rain samples were analyzed for $\delta^{18}O$,
577 with respective mean values of -16.6 and -8.2‰. Soil-water isotopes were not directly
578 measured, but assimilated to precipitation water isotopes. Assuming $\delta^{18}O$ values of
579 air-O_2 of 23.88‰ (Barkan and Luz, 2005), we ended up with $\delta^{18}O\text{-}NO_3^-$ = -3.3‰ (if
580 the end-member is snow water) and +2.3‰ (if the end-member is rain water) for NO_3^-
581 $_{nit}$. Even though this approach comes with a number of assumptions and caveats
582 (Rose et al., 2015b; Snider et al., 2010), the calculated values are significantly higher
583 – by *ca* 4‰ – than the mean annual $\delta^{18}O\text{-}NO_3^-{}_{ter}$ (Table 3). In a study focusing on an
584 estuarine system in San Francisco Bay, it was postulated that rapid recycling of NO_3^-
585 under low [NO_3^-] conditions (<0.9 mg L^{-1}) could result in an increased incorporation of
586 H_2O-O atoms into the NO_3^- molecule (Wankel et al., 2006). Another work focusing on
587 nitrification in forests soils of central Japan attributed low $\delta^{18}O\text{-}NO_3^-$ to a combination
588 of O atoms exchange between H_2O and NO_2^- and kinetic isotope fractionation

589 associated with oxygen incorporation throughout the nitrification process in acidic
590 soils (Fang et al., 2012). The latter hypothesis could explain the generally acidic
591 subalpine soils characterized by slow N cycling (Robson et al., 2007), but further
592 investigation is warranted to understand the cause of ^{18}O depleted NO_3^-.
593 When calculating f_{atm} using the approach described by Barnes et al. (2008):
594
595 (Eq.7) $$f_{atm} = (\delta^{18}O_{sample} - \delta^{18}O_{nit}) / (\delta^{18}O_{atm} - \delta^{18}O_{nit})$$
596
597 and by using either $\delta^{18}O\text{-}NO_3^-_{ter}$ or $\delta^{18}O\text{-}NO_3^-_{nit}$ as nitrification end-member,
598 significant differences between the estimated f_{atm} are obtained (Table 3). These
599 findings suggest that atmospheric NO_3^- inputs to an ecosystem are underestimated
600 (e.g., up to 6% in this study, Table 3) when calculated using Eq.7 with $\delta^{18}O\text{-}NO_3^-_{nit}$ as
601 nitrification end-member.
602
603 **5. Conclusions**
604 The results showing higher $NO_3^-_{atm}$ exports in a montane stream relative to
605 urban streams have several key implications. First, it sheds light on the contribution
606 of snowmelt-derived groundwater to year-round $NO_3^-_{atm}$ exports in all streams at
607 baseflow. Contamination of groundwater by $NO_3^-_{atm}$ may be a widespread
608 phenomenon, regardless of emitting sources proximity: other studies also reported
609 ubiquitous presence of $NO_3^-_{atm}$ in groundwater (Dejwakh et al., 2012; Dietzel et al.,
610 2014; Nakagawa et al., 2013; Stoewer et al., 2015). Second, hydrological events
611 (e.g., snowmelt) are the main controls of upland $NO_3^-_{atm}$ exports, whereas a
612 chemically equilibrated groundwater reservoir dominates discharge in urban streams.
613 In a context of climate change, with temporally shorter and shallower snow coverage

of altitude catchments, decreasing exports of $NO_3^-{}_{atm}$ by snowmelt water could result in proportional $NO_3^-{}_{atm}$ enrichment of alpine soils. However, how this would correlate with elsewhere reported snow cover removal effects on microbial communities, N retention, plants biomass and soil respiration is a complex question yet to be addressed (Brooks et al., 2011; Gavazov et al., 2017; Sorensen et al., 2016; Vankoughnett and Henry, 2013). Third, the association of $\Delta^{17}O$, $\delta^{15}N$ and $\delta^{18}O$ is a potent tool to unravel the respective atmospheric and terrestrial sources contribution to NO_3^- pools. To correct the $\delta^{18}O\text{-}NO_3^-$ from its atmospheric composition enables the determination of the $\delta^{18}O\text{-}NO_3^-{}_{ter}$, which came significantly lower at all sites than the theoretically calculated $\delta^{18}O\text{-}NO_3^-{}_{nit}$. This resulted in significantly higher estimated f_{atm} when using a more robust $\delta^{18}O\text{-}NO_3^-{}_{ter}$ (compared to $\delta^{18}O\text{-}NO_3^-{}_{nit}$) as nitrification end-member in Eq.7. Studies that did not use $\delta^{18}O\text{-}NO_3^-{}_{ter}$ in Eq.7 to determine f_{atm} may have underestimated atmospheric nitrate inputs to the environment (e.g., Barnes et al. (2008), Durka et al. (1994), Griffiths et al. (2016), Pellerin et al. (2012), Sebestyen et al. (2014)). It is recommended that more work be conducted using the triple isotope technique to revise the assessment of $NO_3^-{}_{atm}$ ubiquity in the environment.

Ackowledgments

This study was supported by grants from the Labex OSUG@2020 (“Investissements d’avenir” - ANR10 LABX56), the ARC – Environnement Région Rhone-Alpes, the Grenoble-Chambéry DIPEE CNRS. This work also benefited from the National Research Agency supports (“Investissements d’avenir” - ANR11 INBS-0001AnaEE - Services and “FloodScale project” - ANR 2011 BS56 027) and from the SAJF research station (UMR 3370, UGA-CNRS) infrastructures and competences. The

study took place on a Long Term Ecological Research site of the ZAA (Zone Atelier Alpes) and the Isère Campus monitoring site is a CNRS-labeled site of the ZABR (Rhone Basin Long Term Ecological Research site). We would like to thank G. Nord, J.-L. Jaffrezo, F. Masson, V. Lucaire, E. Vince and C. Arnoldi for help with either laboratory or field work. We also want to acknowledge J. Renaud for help with SIG.

Appendix A

The supplementary information provides additional Text on the analytical methods, Figures S1-S7 and Tables S1-S2.

References

Aber, J.D., Nadelhoffer, K.J., Steudler, P., Melillo, J.M., 1989. Nitrogen Saturation in Northern Forest Ecosystems. BioScience 39, 378–386. https://doi.org/10.2307/1311067

Balestrini, R., Arese, C., Freppaz, M., Buffagni, A., 2013. Catchment features controlling nitrogen dynamics in running waters above the tree line (central Italian Alps). Hydrol. Earth Syst. Sci. 17, 989–1001. https://doi.org/10.5194/hess-17-989-2013

Barkan, E., Luz, B., 2005. High precision measurements of 17O/16O and 18O/16O ratios in H2O. Rapid Commun. Mass Spectrom. 19, 3737–3742. https://doi.org/10.1002/rcm.2250

Barnes, R.T., Raymond, P.A., 2010. Land-use controls on sources and processing of nitrate in small watersheds: insights from dual isotopic analysis. Ecol. Appl. 20, 1961–1978. https://doi.org/10.1890/08-1328.1

Barnes, R.T., Raymond, P.A., Casciotti, K.L., 2008. Dual isotope analyses indicate efficient processing of atmospheric nitrate by forested watersheds in the northeastern US. Biogeochemistry 90, 15–27.

Barnes, R.T., Williams, M.W., Parman, J.N., Hill, K., Caine, N., 2014. Thawing glacial and permafrost features contribute to nitrogen export from Green Lakes Valley, Colorado Front Range, USA. Biogeochemistry 117, 413–430. https://doi.org/10.1007/s10533-013-9886-5

Baron, J.S., Campbell, D.H., 1997. Nitrogen fluxes in a high elevation Colorado Rocky Mountain basin. Hydrol. Process. 11, 783–799.

Baron, J.S., Driscoll, C.T., Stoddard, J.L., Richer, E.E., 2011. Empirical Critical Loads of Atmospheric Nitrogen Deposition for Nutrient Enrichment and Acidification of Sensitive US Lakes. BioScience 61, 602–613. https://doi.org/10.1525/bio.2011.61.8.6

Baron, J.S., Nydick, K.R., Rueth, H.M., Lafrançois, B.M., Wolfe, A.P., 2005. High Elevation Ecosystem Responses to Atmospheric Deposition of Nitrogen in the Colorado Rocky Mountains, USA, in: Huber, U.M., Bugmann, H.K.M., Reasoner, M.A. (Eds.), Global Change and Mountain Regions. Springer Netherlands, Dordrecht, pp. 429–436.

678 Baron, J.S., Rueth, H.M., Wolfe, A.M., Nydick, K.R., Allstott, E.J., Minear, J.T., Moraska, B.,
679 2000. Ecosystem Responses to Nitrogen Deposition in the Colorado Front Range.
680 Ecosystems 3, 352–368. https://doi.org/10.1007/s100210000032
681 Beirle, S., Boersma, K.F., Platt, U., Lawrence, M.G., Wagner, T., 2011. Megacity Emissions
682 and Lifetimes of Nitrogen Oxides Probed from Space. Science 333, 1737–1739.
683 https://doi.org/10.1126/science.1207824
684 Bettez, N.D., Groffman, P.M., 2013. Nitrogen Deposition in and near an Urban Ecosystem.
685 Environ. Sci. Technol. 47, 6047–6051. https://doi.org/10.1021/es400664b
686 Beyn, F., Matthias, V., Dähnke, K., 2014. Changes in atmospheric nitrate deposition in
687 Germany – An isotopic perspective. Environ. Pollut. 194, 1–10.
688 https://doi.org/10.1016/j.envpol.2014.06.043
689 Bodin, X., Thibert, E., Fabre, D., Ribolini, A., Schoeneich, P., Francou, B., Reynaud, L., Fort,
690 M., 2009. Two decades of responses (1986–2006) to climate by the Laurichard rock
691 glacier, French Alps. Permafr. Periglac. Process. 20, 331–344.
692 https://doi.org/10.1002/ppp.665
693 Bourgeois, I., 2017. Atmospheric nitrate deposition on subalpine meadows of the
694 Lautaret pass (phdthesis). Université Grenoble Alpes.
695 Bourgeois, I., Savarino, J., Caillon, N., Angot, H., Barbero, A., Delbart, F., Voisin, D.,
696 Clement, J.-C., n.d. Tracing the fate of atmospheric nitrate in a subalpine watershed using
697 Δ17O. Environ. Sci. Technol. in review.
698 Bowman, W.D., Gartner, J.R., Holland, K., Wiedermann, M., 2006. Nitrogen Critical Loads
699 For Alpine Vegetation And Terrestrial Ecosystem Response: Are We There Yet? Ecol.
700 Appl. 16, 1183–1193. https://doi.org/10.1890/1051-
701 0761(2006)016[1183:NCLFAV]2.0.CO;2
702 Briand, C., 2014. Approche multi-traceurs pour la détermination de l'origine des nitrates
703 dans les eaux souterraines: exemple d'une source karstique dans les Landes. Université
704 Pierre et Marie Curie-Paris VI.
705 Brooks, P.D., Campbell, D.H., Tonnessen, K.A., Heuer, K., 1999. Natural variability in N
706 export from headwater catchments: snow cover controls on ecosystem N retention.
707 Hydrol. Process. 13, 2191–2201.
708 Brooks, P.D., Grogan, P., Templer, P.H., Groffman, P., Öquist, M.G., Schimel, J., 2011.
709 Carbon and Nitrogen Cycling in Snow-Covered Environments. Geogr. Compass 5, 682–
710 699. https://doi.org/10.1111/j.1749-8198.2011.00420.x
711 Burns, D.A., Boyer, E.W., Elliott, E.M., Kendall, C., 2009. Sources and Transformations of
712 Nitrate from Streams Draining Varying Land Uses: Evidence from Dual Isotope Analysis.
713 J. Environ. Qual. 38, 1149. https://doi.org/10.2134/jeq2008.0371
714 Burns, D.A., Kendall, C., 2002. Analysis of δ15N and δ18O to differentiate NO3− sources
715 in runoff at two watersheds in the Catskill Mountains of New York. Water Resour. Res.
716 38, 9–1. https://doi.org/10.1029/2001WR000292
717 Campbell, D.H., Clow, D.W., Ingersoll, G.P., Mast, M.A., Spahr, N.E., Turk, J.T., 1995.
718 Nitrogen deposition and release in alpine watersheds, Loch Vale, Colorado, USA. IAHS
719 Publ.-Ser. Proc. Rep.-Intern Assoc Hydrol. Sci. 228, 243–254.
720 Campbell, D.H., Kendall, C., Chang, C.C.Y., Silva, S.R., Tonnessen, K.A., 2002. Pathways for
721 nitrate release from an alpine watershed: Determination using δ^{15}N and δ^{18}O: ALPINE
722 WATERSHED NITRATE δ^{15}N AND δ^{18}O. Water Resour. Res. 38, 10-1-10–9.
723 https://doi.org/10.1029/2001WR000294
724 Clark, C.M., Bell, M.D., Boyd, J.W., Compton, J.E., Davidson, E.A., Davis, C., Fenn, M.E.,
725 Geiser, L., Jones, L., Blett, T.F., 2017. Nitrogen-induced terrestrial eutrophication:
726 cascading effects and impacts on ecosystem services. Ecosphere 8, e01877.

https://doi.org/10.1002/ecs2.1877
Clément, J.-C., Holmes, R.M., Peterson, B.J., Pinay, G., 2003. Isotopic investigation of denitrification in a riparian ecosystem in western France. J. Appl. Ecol. 40, 1035–1048. https://doi.org/10.1111/j.1365-2664.2003.00854.x
Clow, D.W., Sueker, J.K., 2000. Relations between basin characteristics and stream water chemistry in alpine/subalpine basins in Rocky Mountain National Park, Colorado. Water Resour. Res. 36, 49–61. https://doi.org/10.1029/1999WR900294
Costa, A.W., Michalski, G., Schauer, A.J., Alexander, B., Steig, E.J., Shepson, P.B., 2011. Analysis of atmospheric inputs of nitrate to a temperate forest ecosystem from Δ ^{17} O isotope ratio measurements: ATMOSPHERIC NITRATE INPUTS TO A FOREST. Geophys. Res. Lett. 38, n/a-n/a. https://doi.org/10.1029/2011GL047539
Cowie, R.M., Knowles, J.F., Dailey, K.R., Williams, M.W., Mills, T.J., Molotch, N.P., 2017. Sources of streamflow along a headwater catchment elevational gradient. J. Hydrol. 549, 163–178. https://doi.org/10.1016/j.jhydrol.2017.03.044
Decina, S.M., Templer, P.H., Hutyra, L.R., Gately, C.K., Rao, P., 2017. Variability, drivers, and effects of atmospheric nitrogen inputs across an urban area: Emerging patterns among human activities, the atmosphere, and soils. Sci. Total Environ. 609, 1524–1534. https://doi.org/10.1016/j.scitotenv.2017.07.166
Dejwakh, N.R., Meixner, T., Michalski, G., McIntosh, J., 2012. Using ^{17} O to Investigate Nitrate Sources and Sinks in a Semi-Arid Groundwater System. Environ. Sci. Technol. 46, 745–751. https://doi.org/10.1021/es203450z
Devito, K.J., Fitzgerald, D., Hill, A.R., Aravena, R., 2000. Nitrate dynamics in relation to lithology and hydrologic flow path in a river riparian zone. J. Environ. Qual. 29, 1075–1084.
Dietzel, M., Leis, A., Abdalla, R., Savarino, J., Morin, S., Böttcher, M.E., Köhler, S., 2014. ¹⁷O excess traces atmospheric nitrate in paleo-groundwater of the Saharan desert. Biogeosciences 11, 3149–3161. https://doi.org/10.5194/bg-11-3149-2014
Dodds, W.K., Bouska, W.W., Eitzmann, J.L., Pilger, T.J., Pitts, K.L., Riley, A.J., Schloesser, J.T., Thornbrugh, D.J., 2009. Eutrophication of U.S. Freshwaters: Analysis of Potential Economic Damages. Environ. Sci. Technol. 43, 12–19. https://doi.org/10.1021/es801217q
Durka, W., Schulze, E.-D., Gebauer, G., Voerkeliust, S., 1994. Effects of forest decline on uptake and leaching of deposited nitrate determined from 15N and 18O measurements. Nature 372, 765–767. https://doi.org/10.1038/372765a0
Dutordoir, S., 2014. Bilan des flux de métaux, carbone organique et nutriments contenus dans une rivière alpine: part des rejets urbains de l'agglomération de Grenoble et apports amont (Isère et Drac). Université Grenoble Alpes.
Elliott, E.M., Kendall, C., Boyer, E.W., Burns, D.A., Lear, G.G., Golden, H.E., Harlin, K., Bytnerowicz, A., Butler, T.J., Glatz, R., 2009. Dual nitrate isotopes in dry deposition: Utility for partitioning NO $_x$ source contributions to landscape nitrogen deposition. J. Geophys. Res. 114. https://doi.org/10.1029/2008JG000889
Elser, J.J., Andersen, T., Baron, J.S., Bergström, A.-K., Jansson, M., Kyle, M., Nydick, K.R., Steger, L., Hessen, D.O., 2009. Shifts in lake N:P stoichiometry and nutrient limitation driven by atmospheric nitrogen deposition. Science 326, 835–837. https://doi.org/10.1126/science.1176199
Emmerton, K.S., Callaghan, T.V., Jones, H.E., Leake, J.R., Michelsen, A., Read, D.J., 2001. Assimilation and Isotopic Fractionation of Nitrogen by Mycorrhizal and Nonmycorrhizal Subarctic Plants. New Phytol. 151, 513–524. https://doi.org/10.2307/1353802

776 Erbland, J., 2011. Contraintes isotopiques sur l'interprétation de l'enregistrement en
777 nitrate dans la carotte de glace de Vostok. Université de Grenoble.
778 Estrada, N.L., Böhlke, J.K., Sturchio, N.C., Gu, B., Harvey, G., Burkey, K.O., Grantz, D.A.,
779 McGrath, M.T., Anderson, T.A., Rao, B., Sevanthi, R., Hatzinger, P.B., Jackson, W.A., 2017.
780 Stable isotopic composition of perchlorate and nitrate accumulated in plants:
781 Hydroponic experiments and field data. Sci. Total Environ. 595, 556–566.
782 https://doi.org/10.1016/j.scitotenv.2017.03.223
783 Fang, Y., Koba, K., Makabe, A., Takahashi, C., Zhu, W., Hayashi, T., Hokari, A.A., Urakawa,
784 R., Bai, E., Houlton, B.Z., Xi, D., Zhang, S., Matsushita, K., Tu, Y., Liu, D., Zhu, F., Wang, Z.,
785 Zhou, G., Chen, D., Makita, T., Toda, H., Liu, X., Chen, Q., Zhang, D., Li, Y., Yoh, M., 2015.
786 Microbial denitrification dominates nitrate losses from forest ecosystems. Proc. Natl.
787 Acad. Sci. 112, 1470–1474. https://doi.org/10.1073/pnas.1416776112
788 Fang, Y., Koba, K., Makabe, A., Zhu, F., Fan, S., Liu, X., Yoh, M., 2012. Low δ ^{18} O Values of
789 Nitrate Produced from Nitrification in Temperate Forest Soils. Environ. Sci. Technol. 46,
790 8723–8730. https://doi.org/10.1021/es300510r
791 Fang, Y., Yoh, M., Koba, K., Zhu, W., Takebayashi, Y., Xiao, Y., Lei, C., Mo, J., Zhang, W., Lu,
792 X., 2011. Nitrogen deposition and forest nitrogen cycling along an urban-rural transect
793 in southern China: FOREST N CYCLING IN SOUTHERN CHINA. Glob. Change Biol. 17,
794 872–885. https://doi.org/10.1111/j.1365-2486.2010.02283.x
795 Fowler, D., Steadman, C.E., Stevenson, D., Coyle, M., Rees, R.M., Skiba, U.M., Sutton, M.A.,
796 Cape, J.N., Dore, A.J., Vieno, M., Simpson, D., Zaehle, S., Stocker, B.D., Rinaldi, M., Facchini,
797 M.C., Flechard, C.R., Nemitz, E., Twigg, M., Erisman, J.W., Butterbach-Bahl, K., Galloway,
798 J.N., 2015. Effects of global change during the 21st century onthe nitrogen cycle.
799 Atmospheric Chem. Phys. 15, 13849–13893. https://doi.org/10.5194/acp-15-13849-
800 2015
801 Frey, M.M., Savarino, J., Morin, S., Erbland, J., Martins, J.M.F., 2009. Photolysis imprint in
802 the nitrate stable isotope signal in snow and atmosphere of East Antarctica and
803 implications for reactive nitrogen cycling. Atmospheric Chem. Phys. 9, 8681–8696.
804 Freyer, H.D., 1991. Seasonal variation of 15N/14N ratios in atmospheric nitrate species.
805 Tellus B 43, 30–44. https://doi.org/10.1034/j.1600-0889.1991.00003.x
806 Galloway, J.N., Dentener, F.J., Capone, D.G., Boyer, E.W., Howarth, R.W., Seitzinger, S.P.,
807 Asner, G.P., Cleveland, C.C., Green, P.A., Holland, E.A., Karl, D.M., Michaels, A.F., Porter,
808 J.H., Townsend, A.R., V[?]osmarty, C.J., 2004. Nitrogen Cycles: Past, Present, and Future.
809 Biogeochemistry 70, 153–226. https://doi.org/10.1007/s10533-004-0370-0
810 Galloway, J.N., Townsend, A.R., Erisman, J.W., Bekunda, M., Cai, Z., Freney, J.R., Martinelli,
811 L.A., Seitzinger, S.P., Sutton, M.A., 2008. Transformation of the nitrogen cycle: recent
812 trends, questions, and potential solutions. Science 320, 889–892.
813 Gavazov, K., Ingrisch, J., Hasibeder, R., Mills, R.T.E., Buttler, A., Gleixner, G., Pumpanen, J.,
814 Bahn, M., 2017. Winter ecology of a subalpine grassland: Effects of snow removal on soil
815 respiration, microbial structure and function. Sci. Total Environ. 590–591, 316–324.
816 https://doi.org/10.1016/j.scitotenv.2017.03.010
817 Granger, J., Sigman, D.M., Lehmann, M.F., Tortell, P.D., 2008. Nitrogen and oxygen isotope
818 fractionation during dissimilatory nitrate reduction by denitrifying bacteria. Limnol.
819 Oceanogr. 53, 2533.
820 Granger, J., Sigman, D.M., Needoba, J.A., Harrison, P.J., 2004. Coupled nitrogen and oxygen
821 isotope fractionation of nitrate during assimilation by cultures of marine phytoplankton.
822 Limnol. Oceanogr. 49, 1763–1773.
823 Granger, J., Sigman, D.M., Rohde, M.M., Maldonado, M.T., Tortell, P.D., 2010. N and O
824 isotope effects during nitrate assimilation by unicellular prokaryotic and eukaryotic

plankton cultures. Geochim. Cosmochim. Acta 74, 1030–1040. https://doi.org/10.1016/j.gca.2009.10.044
Granger, J., Wankel, S.D., 2016. Isotopic overprinting of nitrification on denitrification as a ubiquitous and unifying feature of environmental nitrogen cycling. Proc. Natl. Acad. Sci. 113, E6391–E6400. https://doi.org/10.1073/pnas.1601383113
Griffiths, N.A., Jackson, C.R., McDonnell, J.J., Klaus, J., Du, E., Bitew, M.M., 2016. Dual nitrate isotopes clarify the role of biological processing and hydrologic flow paths on nitrogen cycling in subtropical low-gradient watersheds: N CYCLING IN LOW-RELIEF WATERSHEDS. J. Geophys. Res. Biogeosciences 121, 422–437. https://doi.org/10.1002/2015JG003189
Groffman, P.M., Law, N.L., Belt, K.T., Band, L.E., Fisher, G.T., 2004. Nitrogen Fluxes and Retention in Urban Watershed Ecosystems. Ecosystems 7. https://doi.org/10.1007/s10021-003-0039-x
Hall, S.J., Maurer, G., Hoch, S.W., Taylor, R., Bowling, D.R., 2014. Impacts of anthropogenic emissions and cold air pools on urban to montane gradients of snowpack ion concentrations in the Wasatch Mountains, Utah. Atmos. Environ. 98, 231–241. https://doi.org/10.1016/j.atmosenv.2014.08.076
Hall, S.J., Weintraub, S.R., Eiriksson, D., Brooks, P.D., Baker, M.A., Bowen, G.J., Bowling, D.R., 2016. Stream Nitrogen Inputs Reflect Groundwater Across a Snowmelt-Dominated Montane to Urban Watershed. Environ. Sci. Technol. 50, 1137–1146. https://doi.org/10.1021/acs.est.5b04805
Hastings, M.G., Jarvis, J.C., Steig, E.J., 2009. Anthropogenic Impacts on Nitrogen Isotopes of Ice-Core Nitrate. Science 324, 1288–1288. https://doi.org/10.1126/science.1170510
Hertel, O., Skjøth, C.A., Reis, S., Bleeker, A., Harrison, R.M., Cape, J.N., Fowler, D., Skiba, U., Simpson, D., Jickells, T., Kulmala, M., Gyldenkærne, S., Sørensen, L.L., Erisman, J.W., Sutton, M.A., 2012. Governing processes for reactive nitrogen compounds in the European atmosphere. Biogeosciences 9, 4921–4954. https://doi.org/10.5194/bg-9-4921-2012
Holtgrieve, G.W., Schindler, D.E., Hobbs, W.O., Leavitt, P.R., Ward, E.J., Bunting, L., Chen, G., Finney, B.P., Gregory-Eaves, I., Holmgren, S., Lisac, M.J., Lisi, P.J., Nydick, K., Rogers, L.A., Saros, J.E., Selbie, D.T., Shapley, M.D., Walsh, P.B., Wolfe, A.P., 2011. A Coherent Signature of Anthropogenic Nitrogen Deposition to Remote Watersheds of the Northern Hemisphere. Science 334, 1545–1548. https://doi.org/10.1126/science.1212267
Hood, E., Scott, D., 2008. Riverine organic matter and nutrients in southeast Alaska affected by glacial coverage. Nat. Geosci. 1, 583–587. https://doi.org/10.1038/ngeo280
Hundey, E.J., Russell, S.D., Longstaffe, F.J., Moser, K.A., 2016. Agriculture causes nitrate fertilization of remote alpine lakes. Nat. Commun. 7, 10571. https://doi.org/10.1038/ncomms10571
Kaiser, J., Hastings, M.G., Houlton, B.Z., Röckmann, T., Sigman, D.M., 2007. Triple Oxygen Isotope Analysis of Nitrate Using the Denitrifier Method and Thermal Decomposition of N_2O. Anal. Chem. 79, 599–607. https://doi.org/10.1021/ac061022s
Kaye, J.P., Hart, S.C., 1997. Competition for nitrogen between plants and soil microorganisms. Trends Ecol. Evol. 12, 139–143. https://doi.org/10.1016/S0169-5347(97)01001-X
Kean, A.J., Harley, R.A., Littlejohn, D., Kendall, G.R., 2000. On-Road Measurement of Ammonia and Other Motor Vehicle Exhaust Emissions. Environ. Sci. Technol. 34, 3535–3539. https://doi.org/10.1021/es991451q
Kendall, C., Campbell, D.H., Burns, D.A., Shanley, J.B., Silva, S.R., Chang, C.C., 1995. Tracing sources of nitrate in snowmelt runoff using the oxygen and nitrogen isotopic

874 compositions of nitrate. IAHS Publ.-Ser. Proc. Rep.-Intern Assoc Hydrol. Sci. 228, 339–
875 348.
876 Kendall, C., Elliott, E.M., Wankel, S.D., 2007. Tracing anthropogenic inputs of nitrogen to
877 ecosystems. Stable Isot. Ecol. Environ. Sci. 2, 375–449.
878 Kirchner, M., Fegg, W., Römmelt, H., Leuchner, M., Ries, L., Zimmermann, R., Michalke, B.,
879 Wallasch, M., Maguhn, J., Faus-Kessler, T., Jakobi, G., 2014. Nitrogen deposition along
880 differently exposed slopes in the Bavarian Alps. Sci. Total Environ. 470–471, 895–906.
881 https://doi.org/10.1016/j.scitotenv.2013.10.036
882 Lefebvre, S., Clément, J.-C., Pinay, G., Thenail, C., Durand, P., Marmonier, P., 2007. 15n-
883 Nitrate Signature in Low-Order Streams: Effects of Land Cover and Agricultural
884 Practices. Ecol. Appl. 17, 2333–2346. https://doi.org/10.1890/06-1496.1
885 Liu, T., Wang, F., Michalski, G., Xia, X., Liu, S., 2013. Using ^{15} N, ^{17} O, and ^{18} O To Determine
886 Nitrate Sources in the Yellow River, China. Environ. Sci. Technol. 47, 13412–13421.
887 https://doi.org/10.1021/es403357m
888 Liu, X.-Y., Koba, K., Takebayashi, Y., Liu, C.-Q., Fang, Y.-T., Yoh, M., 2013. Dual N and O
889 isotopes of nitrate in natural plants: first insights into individual variability and organ-
890 specific patterns. Biogeochemistry 114, 399–411. https://doi.org/10.1007/s10533-012-
891 9721-4
892 Louiseize, N.L., Lafrenière, M.J., Hastings, M.G., 2014. Stable isotopic evidence of
893 enhanced export of microbially derived $${\text{NO}}_{3}^{ - }$$ NO 3 - following active
894 layer slope disturbance in the Canadian High Arctic. Biogeochemistry 121, 565–580.
895 https://doi.org/10.1007/s10533-014-0023-x
896 Lovett, G.M., Goodale, C.L., 2011. A New Conceptual Model of Nitrogen Saturation Based
897 on Experimental Nitrogen Addition to an Oak Forest. Ecosystems 14, 615–631.
898 https://doi.org/10.1007/s10021-011-9432-z
899 Mano, V., 2008. Processus fondamentaux conditionnant les apports de sediments fins
900 dans les retenues-Optimisation des methodes de mesure et modelisation statistique.
901 Université Joseph-Fourier-Grenoble I.
902 Mano, V., Nemery, J., Belleudy, P., Poirel, A., 2009. Assessment of suspended sediment
903 transport in four alpine watersheds (France): influence of the climatic regime. Hydrol.
904 Process. 23, 777–792. https://doi.org/10.1002/hyp.7178
905 Mara, P., Mihalopoulos, N., Gogou, A., Daehnke, K., Schlarbaum, T., Emeis, K.-C., Krom, M.,
906 2009. Isotopic composition of nitrate in wet and dry atmospheric deposition on Crete in
907 the eastern Mediterranean Sea: ISOTOPIC COMPOSITION OF NITRATE IN DEPOSITION.
908 Glob. Biogeochem. Cycles 23, n/a-n/a. https://doi.org/10.1029/2008GB003395
909 Mast, M.A., Clow, D.W., Baron, J.S., Wetherbee, G.A., 2014. Links between N Deposition
910 and Nitrate Export from a High-Elevation Watershed in the Colorado Front Range.
911 Environ. Sci. Technol. 48, 14258–14265. https://doi.org/10.1021/es502461k
912 Matson, P., Lohse, K.A., Hall, S.J., 2002. The Globalization of Nitrogen Deposition:
913 Consequences for Terrestrial Ecosystems. AMBIO J. Hum. Environ. 31, 113.
914 https://doi.org/10.1639/0044-7447(2002)031[0113:TGONDC]2.0.CO;2
915 Mayer, B., Bollwerk, S.M., Mansfeldt, T., Hütter, B., Veizer, J., 2001. The oxygen isotope
916 composition of nitrate generated by nitrification in acid forest floors. Geochim.
917 Cosmochim. Acta 65, 2743–2756. https://doi.org/10.1016/S0016-7037(01)00612-3
918 Mayer, B., Boyer, E.W., Goodale, C., Jaworski, N.A., Van Breemen, N., Howarth, R.W.,
919 Seitzinger, S., Billen, G., Lajtha, K., Nadelhoffer, K., others, 2002. Sources of nitrate in
920 rivers draining sixteen watersheds in the northeastern US: Isotopic constraints.
921 Biogeochemistry 57, 171–197.
922 Michalski, G., Kolanowski, M., Riha, K.M., 2015. Oxygen and nitrogen isotopic

composition of nitrate in commercial fertilizers, nitric acid, and reagent salts. Isotopes Environ. Health Stud. 51, 382–391. https://doi.org/10.1080/10256016.2015.1054821
Michalski, G., Meixner, T., Fenn, M., Hernandez, L., Sirulnik, A., Allen, E., Thiemens, M., 2004. Tracing Atmospheric Nitrate Deposition in a Complex Semiarid Ecosystem Using Δ17O. Environ. Sci. Technol. 38, 2175–2181. https://doi.org/10.1021/es034980+
Morin, S., Savarino, J., Frey, M.M., Domine, F., Jacobi, H.-W., Kaleschke, L., Martins, J.M.F., 2009. Comprehensive isotopic composition of atmospheric nitrate in the Atlantic Ocean boundary layer from 65°S to 79°N. J. Geophys. Res. 114. https://doi.org/10.1029/2008JD010696
Morin, S., Savarino, J., Frey, M.M., Yan, N., Bekki, S., Bottenheim, J.W., Martins, J.M.F., 2008. Tracing the Origin and Fate of NOx in the Arctic Atmosphere Using Stable Isotopes in Nitrate. Science 322, 730–732. https://doi.org/10.1126/science.1161910
Nakagawa, F., Suzuki, A., Daita, S., Ohyama, T., Komatsu, D.D., Tsunogai, U., 2013. Tracing atmospheric nitrate in groundwater using triple oxygen isotopes: evaluation based on bottled drinking water. Biogeosciences 10, 3547–3558.
Nanus, L., McMurray, J.A., Clow, D.W., Saros, J.E., Blett, T., Gurdak, J.J., 2017. Spatial variation of atmospheric nitrogen deposition and critical loads for aquatic ecosystems in the Greater Yellowstone Area. Environ. Pollut. 223, 644–656. https://doi.org/10.1016/j.envpol.2017.01.077
Nanus, L., Williams, M.W., Campbell, D.H., Elliott, E.M., Kendall, C., 2008. Evaluating Regional Patterns in Nitrate Sources to Watersheds in National Parks of the Rocky Mountains using Nitrate Isotopes. Environ. Sci. Technol. 42, 6487–6493. https://doi.org/10.1021/es800739e
Némery, J., Mano, V., Coynel, A., Etcheber, H., Moatar, F., Meybeck, M., Belleudy, P., Poirel, A., 2013. Carbon and suspended sediment transport in an impounded alpine river (Isère, France). Hydrol. Process. 27, n/a–n/a. https://doi.org/10.1002/hyp.9387
Ohte, N., Sebestyen, S.D., Shanley, J.B., Doctor, D.H., Kendall, C., Wankel, S.D., Boyer, E.W., 2004. Tracing sources of nitrate in snowmelt runoff using a high-resolution isotopic technique: TRACING SOURCES OF NITRATE IN SNOWMELT RUNOFF. Geophys. Res. Lett. 31, n/a-n/a. https://doi.org/10.1029/2004GL020908
Pellerin, B.A., Saraceno, J.F., Shanley, J.B., Sebestyen, S.D., Aiken, G.R., Wollheim, W.M., Bergamaschi, B.A., 2012. Taking the pulse of snowmelt: in situ sensors reveal seasonal, event and diurnal patterns of nitrate and dissolved organic matter variability in an upland forest stream. Biogeochemistry 108, 183–198. https://doi.org/10.1007/s10533-011-9589-8
Preunkert, S., 2003. A seasonally resolved alpine ice core record of nitrate: Comparison with anthropogenic inventories and estimation of preindustrial emissions of NO in Europe. J. Geophys. Res. 108. https://doi.org/10.1029/2003JD003475
Rao, P., Hutyra, L.R., Raciti, S.M., Templer, P.H., 2014. Atmospheric nitrogen inputs and losses along an urbanization gradient from Boston to Harvard Forest, MA. Biogeochemistry 121, 229–245. https://doi.org/10.1007/s10533-013-9861-1
Riha, K.M., Michalski, G., Gallo, E.L., Lohse, K.A., Brooks, P.D., Meixner, T., 2014. High Atmospheric Nitrate Inputs and Nitrogen Turnover in Semi-arid Urban Catchments. Ecosystems 17, 1309–1325. https://doi.org/10.1007/s10021-014-9797-x
Robson, T., Lavorel, S., Clement, J., Roux, X., 2007. Neglect of mowing and manuring leads to slower nitrogen cycling in subalpine grasslands. Soil Biol. Biochem. 39, 930–941. https://doi.org/10.1016/j.soilbio.2006.11.004
Rogora, M., Mosello, R., Arisci, S., Brizzio, M.C., Barbieri, A., Balestrini, R., Waldner, P., Schmitt, M., Stähli, M., Thimonier, A., Kalina, M., Puxbaum, H., Nickus, U., Ulrich, E.,

Probst, A., 2006. An Overview of Atmospheric Deposition Chemistry over the Alps: Present Status and Long-term Trends. Hydrobiologia 562, 17–40. https://doi.org/10.1007/s10750-005-1803-z
Rose, L.A., Elliott, E.M., Adams, M.B., 2015a. Triple Nitrate Isotopes Indicate Differing Nitrate Source Contributions to Streams Across a Nitrogen Saturation Gradient. Ecosystems 18, 1209–1223. https://doi.org/10.1007/s10021-015-9891-8
Rose, L.A., Sebestyen, S.D., Elliott, E.M., Koba, K., 2015b. Drivers of atmospheric nitrate processing and export in forested catchments. Water Resour. Res. 51, 1333–1352. https://doi.org/10.1002/2014WR015716
Sabo, R.D., Nelson, D.M., Eshleman, K.N., 2016. Episodic, seasonal, and annual export of atmospheric and microbial nitrate from a temperate forest: MICROBIAL AND ATMOSPHERIC NITRATE EXPORT. Geophys. Res. Lett. 43, 683–691. https://doi.org/10.1002/2015GL066758
Savarino, J., Kaiser, J., Morin, S., Sigman, D.M., Thiemens, M.H., 2007. Nitrogen and oxygen isotopic constraints on the origin of atmospheric nitrate in coastal Antarctica. Atmospheric Chem. Phys. 7, 1925–1945. https://doi.org/10.5194/acp-7-1925-2007
Sebestyen, S.D., Shanley, J.B., Boyer, E.W., Kendall, C., Doctor, D.H., 2014. Coupled hydrological and biogeochemical processes controlling variability of nitrogen species in streamflow during autumn in an upland forest: STREAM N DYNAMICS DURING AUTUMN. Water Resour. Res. 50, 1569–1591. https://doi.org/10.1002/2013WR013670
Shi, G., Buffen, A.M., Hastings, M.G., Li, C., Ma, H., Li, Y., Sun, B., An, C., Jiang, S., 2015. Investigation of post-depositional processing of nitrate in East Antarctic snow: isotopic constraints on photolytic loss, re-oxidation, and source inputs. Atmospheric Chem. Phys. 15, 9435–9453. https://doi.org/10.5194/acp-15-9435-2015
Snider, D.M., Spoelstra, J., Schiff, S.L., Venkiteswaran, J.J., 2010. Stable Oxygen Isotope Ratios of Nitrate Produced from Nitrification: 18O-Labeled Water Incubations of Agricultural and Temperate Forest Soils. Environ. Sci. Technol. 44, 5358–5364. https://doi.org/10.1021/es1002567
Sorensen, P.O., Templer, P.H., Christenson, L., Duran, J., Fahey, T., Fisk, M.C., Groffman, P.M., Morse, J.L., Finzi, A.C., 2016. Reduced snow cover alters root-microbe interactions and decreases nitrification rates in a northern hardwood forest. Ecology 97, 3359–3368. https://doi.org/10.1002/ecy.1599
Spoelstra, J., Schiff, S.L., Hazlett, P.W., Jeffries, D.S., Semkin, R.G., 2007. The isotopic composition of nitrate produced from nitrification in a hardwood forest floor. Geochim. Cosmochim. Acta 71, 3757–3771. https://doi.org/10.1016/j.gca.2007.05.021
Stoewer, M.M., Knöller, K., Stumpp, C., 2015. Tracing freshwater nitrate sources in pre-alpine groundwater catchments using environmental tracers. J. Hydrol. 524, 753–767. https://doi.org/10.1016/j.jhydrol.2015.03.022
Templer, P.H., Weathers, K.C., 2011. Use of mixed ion exchange resin and the denitrifier method to determine isotopic values of nitrate in atmospheric deposition and canopy throughfall. Atmos. Environ. 45, 2017–2020. https://doi.org/10.1016/j.atmosenv.2011.01.035
Templer, P.H., Weathers, K.C., Lindsey, A., Lenoir, K., Scott, L., 2015. Atmospheric inputs and nitrogen saturation status in and adjacent to Class I wilderness areas of the northeastern US. Oecologia 177, 5–15. https://doi.org/10.1007/s00442-014-3121-5
Thiemens, M.H., 2006. History and applications of mass-independent isotope effects. Annu Rev Earth Planet Sci 34, 217–262.
Tomaz, S., Jaffrezo, J.-L., Favez, O., Perraudin, E., Villenave, E., Albinet, A., 2017. Sources and atmospheric chemistry of oxy- and nitro-PAHs in the ambient air of Grenoble

(France). Atmos. Environ. 161, 144–154. https://doi.org/10.1016/j.atmosenv.2017.04.042
Treibergs, L.A., Granger, J., 2017. Enzyme level N and O isotope effects of assimilatory and dissimilatory nitrate reduction: Enzyme level N and O isotope effects. Limnol. Oceanogr. 62, 272–288. https://doi.org/10.1002/lno.10393
Tsunogai, U., Komatsu, D.D., Daita, S., Kazemi, G.A., Nakagawa, F., Noguchi, I., Zhang, J., 2010. Tracing the fate of atmospheric nitrate deposited onto a forest ecosystem in Eastern Asia using Δ 17 O. Atmospheric Chem. Phys. 10, 1809–1820.
Tsunogai, U., Komatsu, D.D., Ohyama, T., Suzuki, A., Nakagawa, F., Noguchi, I., Takagi, K., Nomura, M., Fukuzawa, K., Shibata, H., 2014. Quantifying the effects of clear-cutting and strip-cutting on nitrate dynamics in a forested watershed using triple oxygen isotopes as tracers. Biogeosciences 11, 5411–5424. https://doi.org/10.5194/bg-11-5411-2014
Tsunogai, U., Miyauchi, T., Ohyama, T., Komatsu, D.D., Nakagawa, F., Obata, Y., Sato, K., Ohizumi, T., 2016. Accurate and precise quantification of atmospheric nitrate in streams draining land of various uses by using triple oxygen isotopes as tracers. Biogeosciences 13, 3441–3459. https://doi.org/10.5194/bg-13-3441-2016
Vankoughnett, M.R., Henry, H.A.L., 2013. Combined Effects of Soil Freezing and N Addition on Losses and Interception of N Over Winter and Summer. Ecosystems 16, 694–703. https://doi.org/10.1007/s10021-013-9642-7
Vitousek, P.M., Aber, J.D., Howarth, R.W., Likens, G.E., Matson, P.A., Schindler, D.W., Schlesinger, W.H., Tilman, D.G., 1997. HUMAN ALTERATION OF THE GLOBAL NITROGEN CYCLE: SOURCES AND CONSEQUENCES. Ecol. Appl. 7, 737–750. https://doi.org/10.1890/1051-0761(1997)007[0737:HAOTGN]2.0.CO;2
Wankel, S.D., Kendall, C., Francis, C.A., Paytan, A., 2006. Nitrogen sources and cycling in the San Francisco Bay Estuary: A nitrate dual isotopic composition approach. Limnol. Oceanogr. 51, 1654–1664.
Wasiuta, V., Lafrenière, M.J., Norman, A.-L., Hastings, M.G., 2015. Summer deposition of sulfate and reactive nitrogen to two alpine valleys in the Canadian Rocky Mountains. Atmos. Environ. 101, 270–285. https://doi.org/10.1016/j.atmosenv.2014.10.041
Weijs, S.V., Mutzner, R., Parlange, M.B., 2013. Could electrical conductivity replace water level in rating curves for alpine streams?: ELECTRICAL CONDUCTIVITY STREAMFLOW RATING CURVES. Water Resour. Res. 49, 343–351. https://doi.org/10.1029/2012WR012181
Wexler, S.K., Goodale, C.L., McGuire, K.J., Bailey, S.W., Groffman, P.M., 2014. Isotopic signals of summer denitrification in a northern hardwood forested catchment. Proc. Natl. Acad. Sci. 111, 16413–16418. https://doi.org/10.1073/pnas.1404321111
Williams, J.J., Nurse, A., Saros, J.E., Riedel, J., Beutel, M., 2016. Effects of glaciers on nutrient concentrations and phytoplankton in lakes within the Northern Cascades Mountains (USA). Biogeochemistry 131, 373–385. https://doi.org/10.1007/s10533-016-0264-y
Williams, M.W., Knauf, M., Cory, R., Caine, N., Liu, F., 2007. Nitrate content and potential microbial signature of rock glacier outflow, Colorado Front Range. Earth Surf. Process. Landf. 32, 1032–1047. https://doi.org/10.1002/esp.1455
Williams, M.W., Melack, J.M., 1991. Solute chemistry of snowmelt and runoff in an Alpine Basin, Sierra Nevada. Water Resour. Res. 27, 1575–1588. https://doi.org/10.1029/90WR02774
Williams, M.W., Seibold, C., Chowanski, K., 2009. Storage and release of solutes from a subalpine seasonal snowpack: soil and stream water response, Niwot Ridge, Colorado. Biogeochemistry 95, 77–94. https://doi.org/10.1007/s10533-009-9288-x

Yang, Y.-Y., Toor, G.S., 2016. δ ^{15}N and δ ^{18}O Reveal the Sources of Nitrate-Nitrogen in Urban Residential Stormwater Runoff. Environ. Sci. Technol. https://doi.org/10.1021/acs.est.5b05353
Ye, C., Gao, H., Zhang, N., Zhou, X., 2016. Photolysis of Nitric Acid and Nitrate on Natural and Artificial Surfaces. Environ. Sci. Technol. 50, 3530–3536. https://doi.org/10.1021/acs.est.5b05032

Watershed	S-upper montane	N-upper montane	Mid montane	Lower montane	Upper urban	Lower Urban
Main regime	Snowmelt	Glacier melt	Snowmelt	Snowmelt	Snowmelt - Rainfall	Snowmelt - Rainfall
Altitude range (m a.s.l.)	1667-2725	1667-3155	1618-1980	1050-4088	210-2650	210-4088
Size (km^2)	3.4	5.3	0.5	220	5720	3600
Mean slope (%)	25	30	17	28	22	22
Geology	Calcareous	Granitic and ancient volcanic rocks	Calcareous	60% Marls and carbonates, 40% Metamorphic and crystalline rocks	77% Marls and carbonates, 15% Metamorphic and crystalline rocks, 8% glacial deposits	Crystalline rocks (granite, gneiss and amphibolite)
Land cover	30% alpine meadows (grazed), 27% uncovered, 26% abandoned grasslands, 13% terraced meadows (mown for hay), some habitations	Mostly uncovered and abandoned grasslands	80% terraced meadows (mown for hay), 13% alpine meadows, one village	60% Uncovered, 40% Forest or low vegetation, a few villages	74% Forest and semi-natural vegetation, 22% Agricultural fields, 4% Urbanized areas	81% Forest and semi-natural vegetation, 16% Agricultural fields, 3% urbanized areas

Table 1 Characteristics of the Romanche Valley and Isere watersheds along the montane to urban gradient

1115

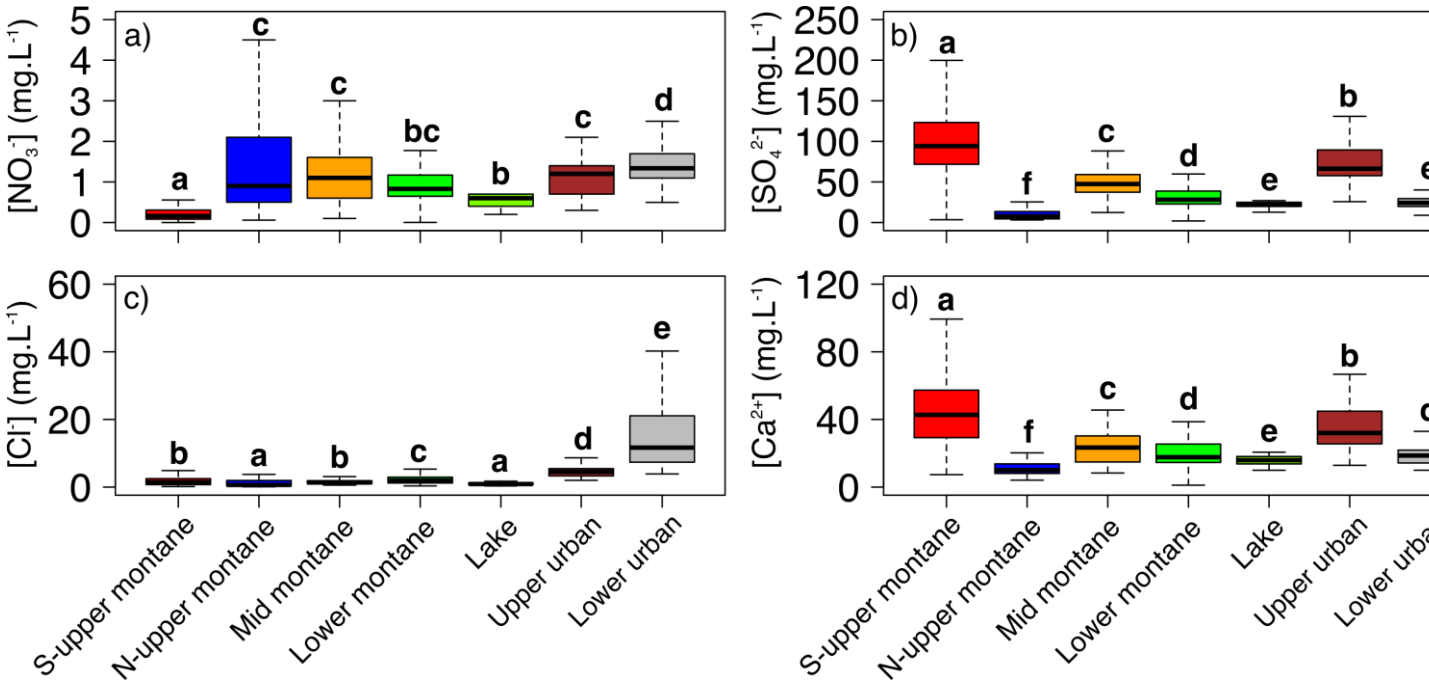

Figure 1 Two years solute concentrations in streams, with a) $[NO_3^-]$ (mg L^{-1}), b) $[SO_4^{2-}]$ (mg L^{-1}), c) $[Cl^-]$ (mg L^{-1}) and d) $[Ca^{2+}]$ (mg L^{-1}). Different letters denote significant differences in NO_3^- isotopic composition across sites. (e.g., a site with *ab* letters is significantly different from sites with letters from *c* onwards, but not significantly different from sites with *a* or *b* letters).

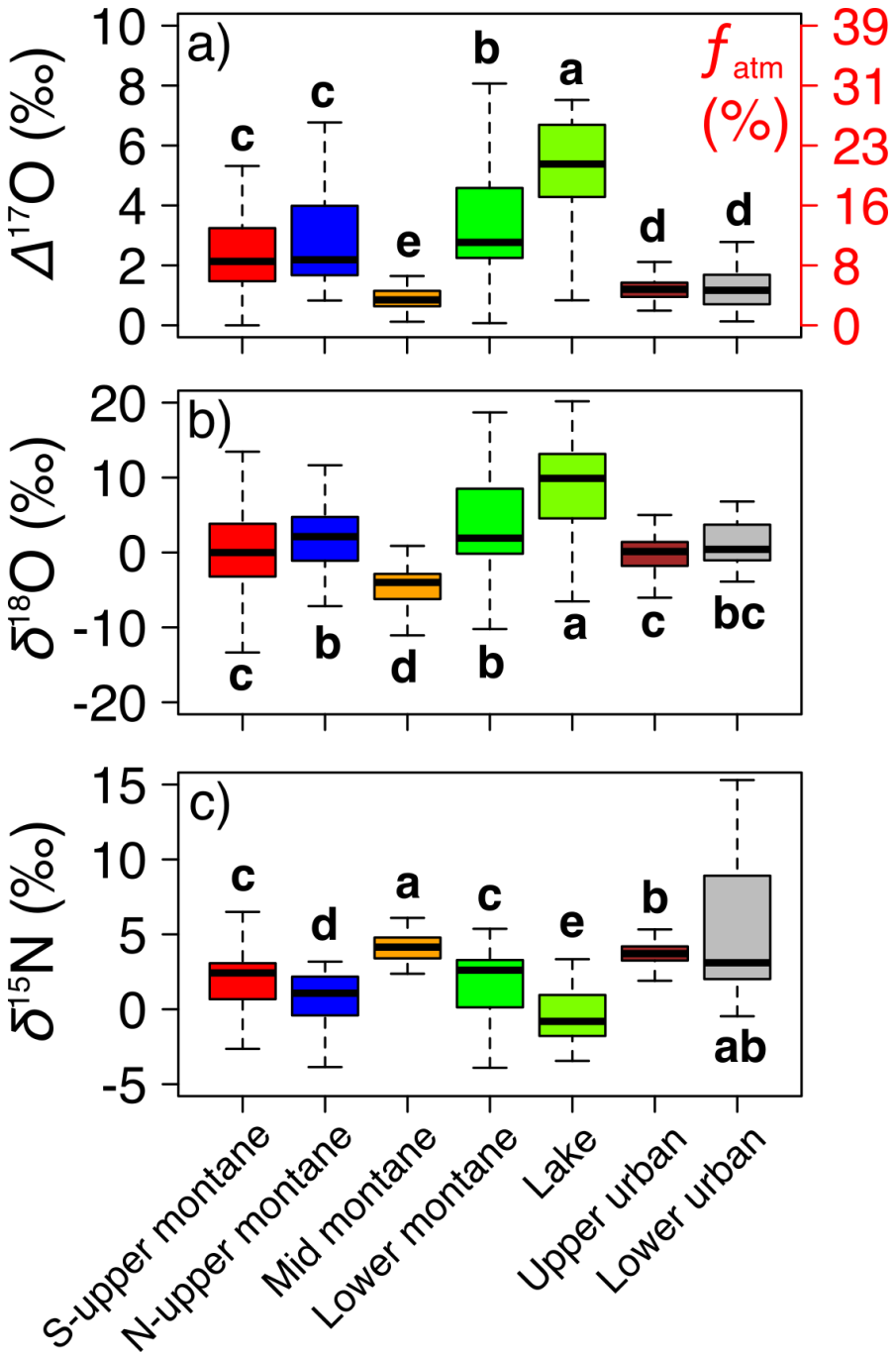

Figure 2 Two years isotopic composition of NO_3^- in streams, with a) $\Delta^{17}O$ (‰) (and corresponding f_{atm} (%) on the red y-axis), b) $\delta^{18}O$ (‰) and c) $\delta^{15}N$ (‰). Different letters denote significant differences in NO_3^- isotopic composition among sites (e.g., a site with *ab* letters is significantly different from sites with letters from *c* onwards, but not significantly different from sites with *a* or *b* letters).

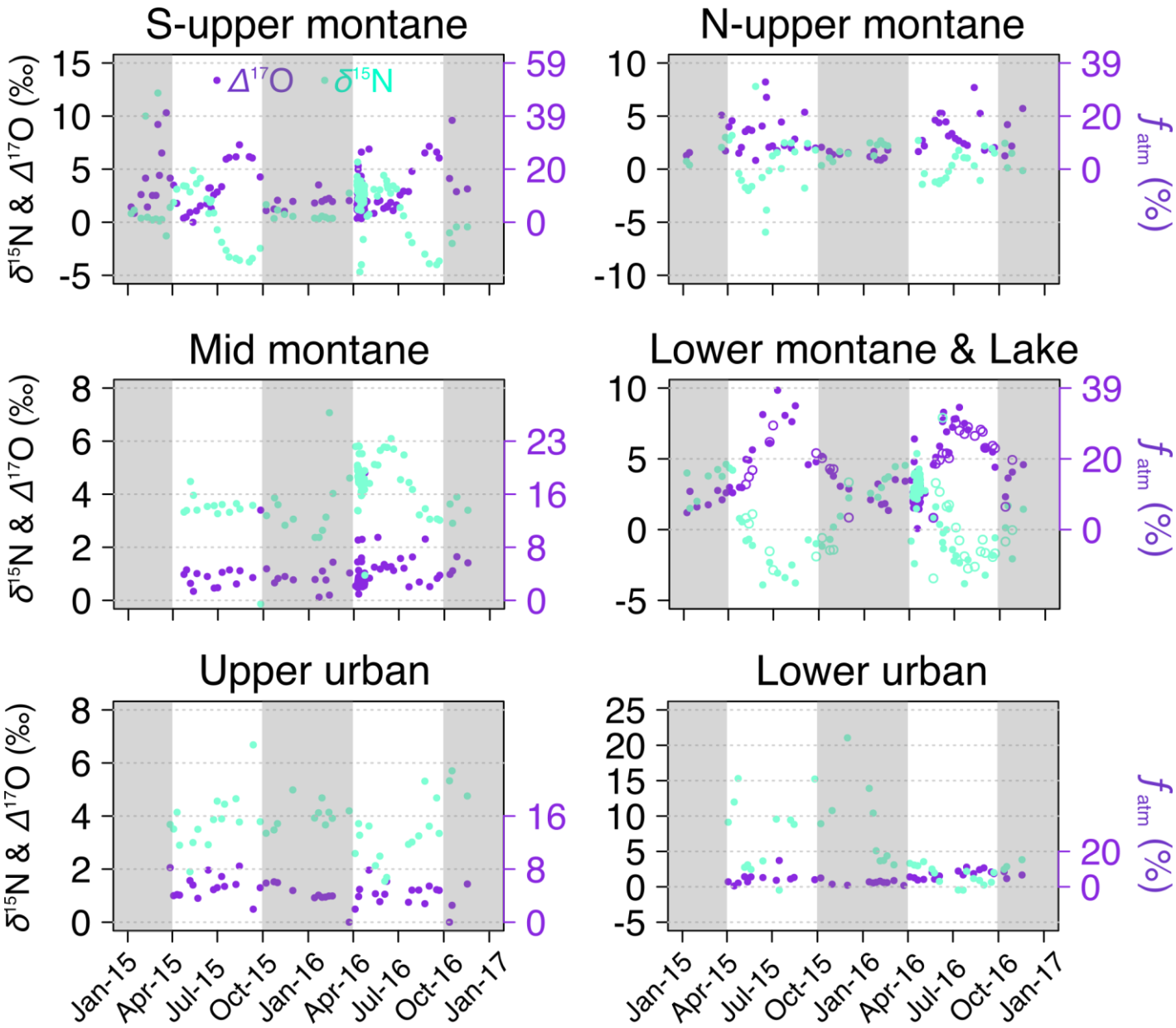

Figure 3 Seasonal variations of $\Delta^{17}O\text{-}NO_3^-$ and $\delta^{15}N\text{-}NO_3^-$(‰) in streams. Point colors denote isotopes as indicated in legend. Range of corresponding f_{atm} (%) is indicated on the secondary y-axis. on the red y-axis). Highlighted in grey is the dormant season (October-April). Note the different y-axes scales across the different panels.

	Mean discharge-weighted annual $[NO_3^-]$ (mgL^{-1})		Mean discharge weighted f_{atm} (%) based on $\Delta^{17}O$ (‰)		Total NO_3^- flux (kg N ha^{-1} yr^{-1})		Total $NO_3^-{}_{atm}$ flux (kg N ha^{-1} yr^{-1})	
	2015	2016	2015	2016	2015	2016	2015	2016
Lower montane	1.0	0.9	22	19	1.9	1.4	0.4	0.3
Upper urban	1.0	1.2	5	4	2.0	2.6	0.1	0.1
Lower urban	1.7	1.3	4	5	4.8	2.1	0.2	0.1

Table 2 Mean discharge-weighted annual $[NO_3^-]$ and associated (mgL^{-1}) and f_{atm} (%), annual fluxes of total NO_3^- and total $NO_3^-{}_{atm}$ in streams and deduced annual contribution of $NO_3^-{}_{atm}$ yield to the total NO_3^-flux at three sites along the montane to urban gradient for years 2015 and 2016.

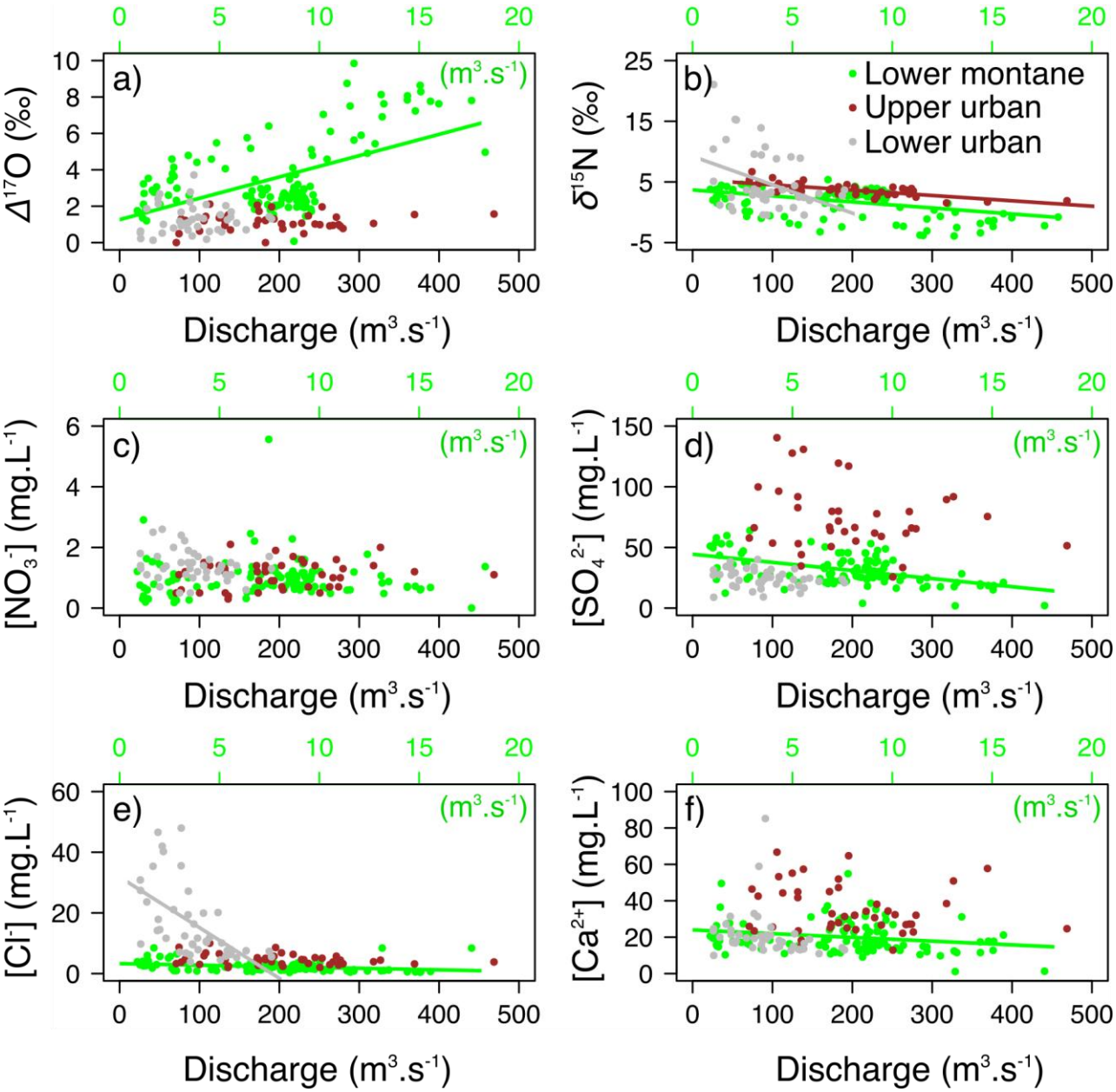

Figure 4 Relationships of nitrate isotopes and solutes concentration with discharge at three sites along the montane to urban gradient. Linear correlations were plotted only if significant. Note the differences in the y-axis scales among the panels, and the specific x-axis for discharge at the lower montane site (in green). Point colors denote sites as indicated in legend.

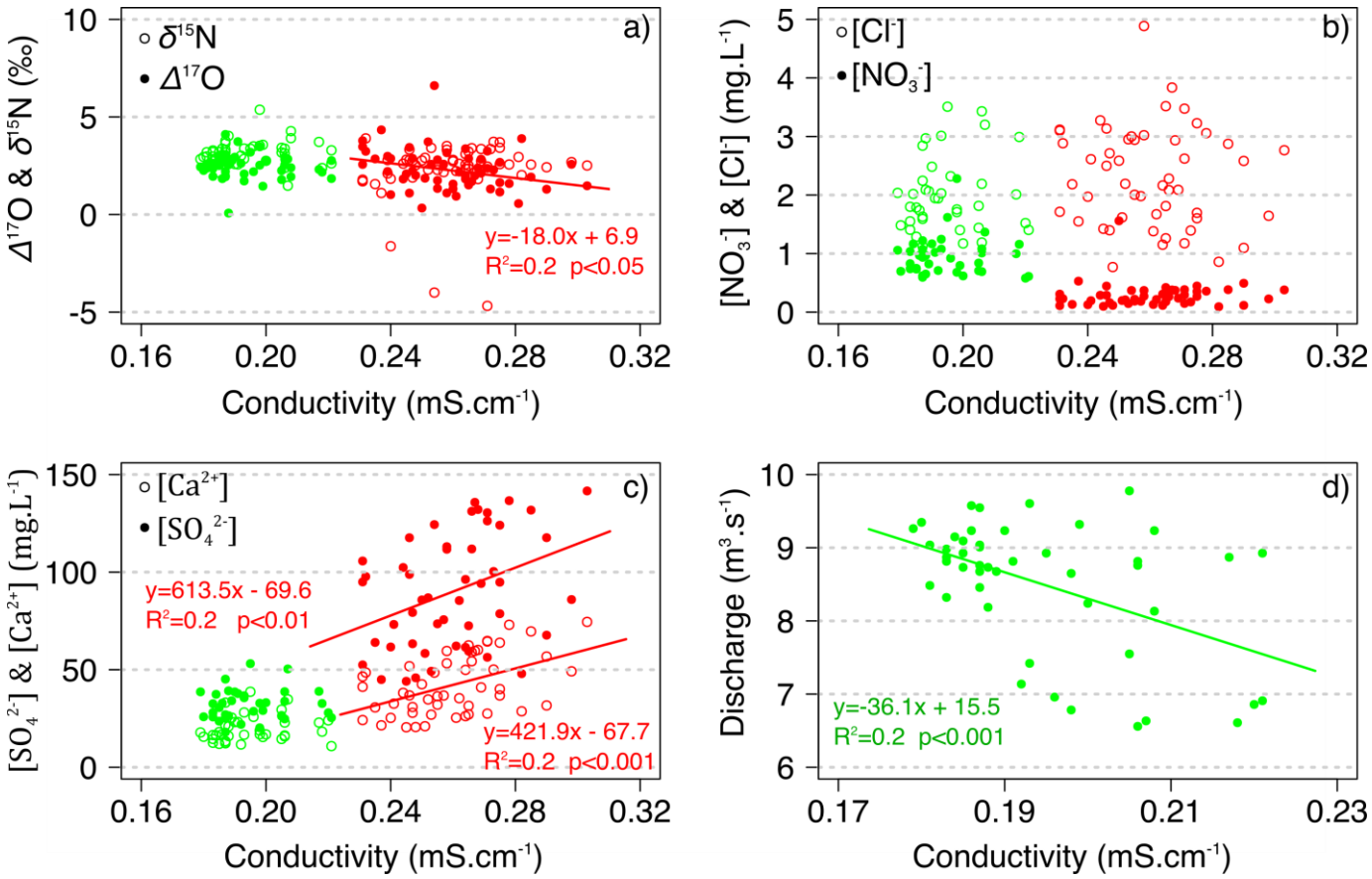

Figure 5 Relationships of NO_3^- isotopes, solute concentration and discharge with conductivity during snowmelt (April 8 to April 24 in 2016) at the S-upper montane (in red) and the lower montane (in green) sites. Linear regressions were plotted only if significant. Full or open circles feature either a) different NO_3^- isotopes or b) and c) different solute concentrations.

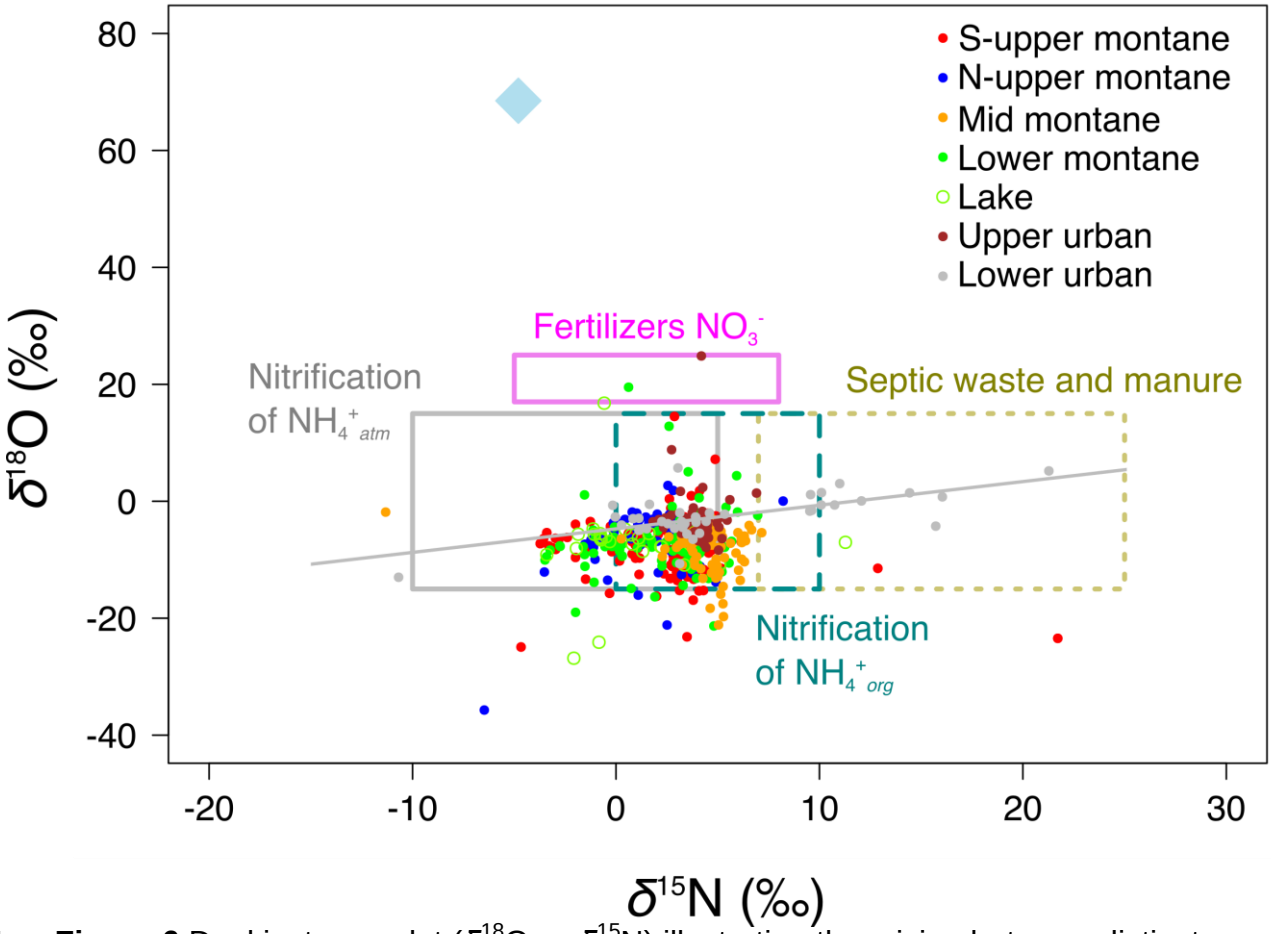

Figure 6 Dual isotopes plot ($\delta^{18}O$ *vs* $\delta^{15}N$) illustrating the mixing between distinct sources of $NO_3^-{}_{ter}$ (non-atmospheric) in streams. All isotopic values were obtained by the $\Delta^{17}O$ transform of NO_3^- collected at all sites (see *Methods*). The colored boxes represent the reported range for NO_3^- terrestrial sources, featuring atmospheric ammonium ($NH_4^+{}_{atm}$) in grey, mineralized ammonium ($NH_4^+{}_{org}$) in turquoise, manure or sewage derived NH_4^+ in beige and fertilizers NO_3^- in violet (Kendall et al., 2007). Linear regressions were plotted only when significant. The blue diamond reflects the isotopic composition of $NO_3^-{}_{atm}$ as measured in this study. Point colors denote sites as indicated in legend.

	Mean annual $\delta^{18}O\text{-}NO_3^-$ (‰)	Mean annual $\delta^{18}O\text{-}NO_{3\ ter}^-$(‰)and *deduced % $NO_{3\ atm}^-$*	Calculated $\delta^{18}O\text{-}NO_{3\ nit}^-$ (‰) and *deduced % $NO_{3\ atm}^-$*
S-upper montane	0.7± 6.6	-7.7 ± 4.8*11* ± *7*[a]	-3.3 ± 3.4*5* ± *9*[b]
N-uppermontane	2.8 ±4.2	-6.3 ± 5.6*12* ± *7*[a]	-3.3 ± 3.4*8* ± *6*[b]
Mid-montane	-4.9 ± 4.1	-8.0 ± 3.7***4 ± 3***[a]	-3.3 ± 3.4***0 ± 5***[b]
Lower montane	4.1 ± 6.6	-6.8 ± 6.7*14* ± *8*[a]	-3.3 ± 3.4*10* ± *9*[b]
Lake	8.6 ± 6.2	-7.3 ± 4.8*20* ± *7*[a]	-3.3 ± 3.4*16* ± *8*[a]
Upper urban	0.9 ± 5.7	-2.8 ± 5.3***5 ± 2***[a]	2.3 ± 4.2***0 ± 4***[b]
Lower urban	1.1 ± 3.8	-2.6 ± 3.5***5 ± 3***[a]	2.3 ± 4.2***0 ± 6***[b]

Table 3 The second column gives the mean annual $\delta^{18}O\text{-}NO_3^-$ (‰) measured in streams. The third column shows the mean annual $\delta^{18}O\text{-}NO_{3\ ter}^-$ (‰) after samples isotopic composition was corrected for the atmospheric imprint (see *Methods*), and the corresponding proportion of $NO_{3\ atm}^-$ when using the corrected value as microbial end-member. Fourth column presents the calculated theoretical $\delta^{18}O\text{-}NO_{3\ nit}^-$ when using the approach detailed in section 4.3, and the corresponding proportion of $NO_{3\ atm}^-$ when using this theoretical value as microbial end-member. Superscript letters indicate significant differences in the proportion of $NO_{3\ atm}^-$ inferred by both methods ($p < 0.05$).